THE JOURNAL OF BIOLOGICAL CHEMISTRY VOL. 291, NO. 28, pp. 14639–14661, July 8, 2016
Published in the U.S.A.

Mutants of Cytochrome P450 Reductase Lacking Either Gly-141 or Gly-143 Destabilize Its FMN Semiquinone*[S]

Received for publication, February 29, 2016, and in revised form, April 26, 2016 Published, JBC Papers in Press, May 9, 2016, DOI 10.1074/jbc.M116.724625

Freeborn Rwere[‡1], Chuanwu Xia[§1], Sangchoul Im[‡], Mohammad M. Haque[¶], Dennis J. Stuehr[¶], Lucy Waskell[‡2], and Jung-Ja P. Kim[§3]

From the [‡]Department of Anesthesiology, University of Michigan and Veterans Affairs Medical Center, Ann Arbor, Michigan 48105, the [§]Department of Biochemistry, Medical College of Wisconsin, Milwaukee, Wisconsin 53226, and the [¶]Department of Pathobiology, Lerner Research Institute, Cleveland Clinic, Cleveland, Ohio 44195

NADPH-cytochrome P450 oxidoreductase transfers electrons from NADPH to cytochromes P450 via its FAD and FMN. To understand the biochemical and structural basis of electron transfer from FMN-hydroquinone to its partners, three deletion mutants in a conserved loop near the FMN were characterized. Comparison of oxidized and reduced wild type and mutant structures reveals that the basis for the air stability of the neutral blue semiquinone is protonation of the flavin N5 and strong H-bond formation with the Gly-141 carbonyl. The ΔGly-143 protein had moderately decreased activity with cytochrome P450 and cytochrome *c*. It formed a flexible loop, which transiently interacts with the flavin N5, resulting in the generation of both an unstable neutral blue semiquinone and hydroquinone. The ΔGly-141 and ΔG141/E142N mutants were inactive with cytochrome P450 but fully active in reducing cytochrome *c*. In the ΔGly-141 mutants, the backbone amide of Glu/Asn-142 forms an H-bond to the N5 of the oxidized flavin, which leads to formation of an unstable red anionic semiquinone with a more negative potential than the hydroquinone. The semiquinone of ΔG141/E142N was slightly more stable than that of ΔGly-141, consistent with its crystallographically demonstrated more rigid loop. Nonetheless, both ΔGly-141 red semiquinones were less stable than those of the corresponding loop in cytochrome P450 BM3 and the neuronal NOS mutant (ΔGly-810). Our results indicate that the catalytic activity of cytochrome P450 oxidoreductase is a function of the length, sequence, and flexibility of the 140s loop and illustrate the sophisticated variety of biochemical mechanisms employed in fine-tuning its redox properties and function.

Flavin-containing enzymes are abundant and occur in all kingdoms of life. A staggering array of versatile redox reactions is catalyzed by flavin-containing oxidases, oxygenases, dehydrogenases, and electron transfer proteins that occur in essential biochemical systems and pathways, including but not limited to photosynthesis, respiration, light-activated signal transduction, bacterial cell wall synthesis, DNA synthesis and repair, magnetic sensing, chemiluminescence, photomorphogenesis, and regulation of circadian rhythms (1–4). The extraordinary chemical versatility of flavins provides metabolic economy, which means that only a few different cofactors are necessary to accomplish the biochemical reactions required for life (5, 6). However, it also follows that individual enzymes and proteins must select cofactor chemistry that is appropriate for the task at hand while suppressing many of the intrinsic reactivities of the flavin. An interesting but unanswered question is as follows. How do the interactions between the protein and the isoalloxazine ring modify and regulate the innate chemistry of the flavin and adapt it to a specific biochemical reaction?

The flavin isoalloxazine ring can exist in the following three different oxidation states: oxidized (ox),[4] one-electron reduced semiquinone (sq), and a two-electron reduced hydroquinone (hq). The semiquinone radical has two forms. One is red and anionic; the other is blue and neutral, with protonation of the flavin N5, whose pK_a is 8.5. N1 of the free flavin hydroquinone has a pK_a of ~6.7, and as a result, it is assumed to exist as the anionic form in proteins at physiologic pH (7–10). Each of these redox/ionic forms can also exist as resonance hybrids or in a charge-transfer complex (5). The N1, C4a, and N5 atoms of the enediamine group of the flavins are primarily involved in the reversible one- and two-electron transfer reactions of the flavin (6). The oxidized flavin is an electron-deficient and highly conjugated three-membered ring roughly composed of a xylene, a pyrazine, and a pyrimidine ring. The electrostatic potential of the isoalloxazine ring is most negative at the O2 and O4 of the pyrimidine (11). As a result, flavins can accept/donate either one or two electrons. This unique property enables flavoproteins to be a mediator between two-electron carriers (*e.g.* pyridine nucleotides NAD^+/$NADP^+$) and one-electron carriers (*e.g.* heme) in oxidation-reduction reactions and electron transfer processes, thereby providing great versatility in various

* This work was supported by National Institutes of Health Grants GM035533 and GM094209, a Veterans Affairs Merit review grant (to L. W.), and National Institutes of Health Grants GM097031 (to J. J. K.) and GM51491 (to D. J. S.). The authors declare that they have no conflicts of interest with the contents of this article. The content is solely the responsibility of the authors and does not necessarily represent the official views of the National Institutes of Health.

[S] This article contains supplemental Figs. S1–S4 and video 1.

The atomic coordinates and structure factors (codes 4YAF, 4YAL, 4Y9R, 4YAW, 4Y7C, 4YAU, 4Y9U, and 4YAO) have been deposited in the Protein Data Bank (http://wwpdb.org/).

[1] Both authors contributed equally to this work.

[2] To whom correspondence may be addressed: Dept. of Anesthesiology Research, University of Michigan Medical School, 2215 Fuller Rd., Bldg. 31, Ann Arbor, MI 48105. Tel.: 734-845-5858; Fax: 734-845-3096; E-mail: waskell@umich.edu.

[3] To whom correspondence may be addressed: Dept. of Biochemistry, Medical College of Wisconsin, 8701 Watertown Plank Rd., Milwaukee, WI 53226. Tel.: 414-955-8479; Fax: 414-955-6510; E-mail: jjkim@mcw.edu.

[4] The abbreviations used are: ox, oxidized; sq, semiquinone; hq, hydroquinone; CYPOR, cytochrome P450 oxidoreductase; cyt *c*, cytochrome *c*; PDB, Protein Data Bank; nNOS, neuronal NOS.

chemical reactions. Flavoproteins employ hydrogen bonding, microscopic dielectric constants, polarity, placement of local charges, and π aromatic stacking interactions (which are mediated by dispersion and electrostatic forces) with the flavin to selectively stabilize a particular oxidation state and thereby provide the enzyme with the ability to control the cofactor redox potential and ultimately enzymatic function (12). In addition to tuning the thermodynamics of the reaction, flavoproteins also kinetically regulate electron transfer by influencing the rate of proton transfer (3).

Microsomal NADPH-cytochrome P450 oxidoreductase (CYPOR) is the prototype of the diflavin reductase family, containing both FMN and FAD, that provides electrons to the superfamily of microsomal cytochromes P450 (10, 13–17), heme oxygenase (18), and cytochrome b_5 (19). The ~50 microsomal cytochrome P450s in humans catalyze the oxidation of a wide variety of essential endogenous and exogenous compounds. FAD receives electrons from the obligate two-electron donor, NADPH, and transfers the electrons one at a time to FMN, which is the electron donor to its one-electron acceptor redox partners (20, 21). The FMN domain is homologous to flavodoxins, whereas the FAD domain is similar to ferredoxin-$NADP^+$ oxidoreductase. Because of the remarkable conservation of the sequence between these two proteins and CYPOR, it has been proposed that CYPOR and the diflavin reductase family evolved as a result of the fusion between these two ancestral proteins (22). In addition to CYPOR, the diflavin oxidoreductase family includes the reductase domains of nitric-oxide synthase (NOS) isozymes, flavocytochrome P450 from *Bacillus megaterium* (P450 BM3), sulfite reductase, and methionine synthase reductase (10).

It is the low potential FMN hq of the amphipathic full-length CYPOR that transfers a total of two electrons, one at a time, initially to ferric cyt P450 and later, in the catalytic cycle, to oxyferrous cyt P450 (10). The high potential of the FMN semiquinone forms an air-stable, protonated, neutral blue semiquinone that is not capable of transferring electrons to the ferric heme of cyt P450. Although the structures of the FMN domains of CYPOR and P450 BM3 are very similar, their FMN domains exhibit very different redox properties (20, 23–29). It is the one-electron-reduced, red anionic, low potential FMN semiquinone in P450BM3 that is capable of very rapidly (~280 s^{-1}) reducing the ferric heme rather than the FMN hydroquinone, which has a more positive potential incapable of reducing the ferric heme. What accounts for the reversal of the semiquinone and hydroquinone potentials in CYPOR and the P450BM3 reductase? The major structural difference between the FMN domains of CYPOR and the BM3 reductase is the lack of a highly conserved glycine residue (Gly-141 in rat CYPOR) in a loop in contact with the re-face of the isoalloxazine ring (24). Another difference is that CYPOR and flavodoxins possess a more negative electrostatic environment around the N1 atom of the FMN ring compared with the BM3 reductase domain. The less negative and more hydrophobic environment around the FMN in the P450 BM3 reductase contributes to a more positive potential for the anionic FMN hydroquinone in the BM3 reductase (24, 30).

In the NOS reductase domain and flavodoxins, a conserved glycine carbonyl oxygen forms an H-bond with the protonated N5 of the semiquinone resulting in an air-stable, neutral blue, high potential semiquinone that does not support catalysis in their redox partners (26, 28, 31–35). In contrast, in the P450 BM3 reductase domain, the N5 of the oxidized FMN forms an H-bond with the main chain amide nitrogen of Asn-537, which prevents protonation of the flavin semiquinone and gives rise to an anionic low potential semiquinone capable of reducing the heme. In flavodoxins, protonation of the flavin N5 is possible because a flexible loop in flavodoxins is free to rotate up toward the NH5 of the FMN semiquinone and forms a stabilizing H-bond between it and the carbonyl of the conserved glycine (Gly-141 in CYPOR). Shortening the loop in NOS reductase by removing the conserved glycine results in a protein with redox properties similar to those of the BM3 reductase (negative oxidized/semiquinone and positive semiquinone/hydroquinone potentials). In contrast, engineering an additional glycine into the loop in the P450 BM3 reductase produces a mutant with redox properties similar to those of CYPOR, flavodoxins, and NOS reductase (positive oxidized/semiquinone and negative semiquinone/hydroquinone potentials) (25, 36).

As discussed above, although the role of glycines homologous to Gly-141 in CYPOR has been studied in other flavoproteins, the structure and function of the conserved Gly-141 have not been investigated in CYPOR. Moreover, there is another conserved glycine, Gly-143, in the loop spanning residues 139–146 (hereafter referred to as the "140s" loop) of CYPOR. Because of its proximity to the flavin and its conservation in similar proteins, it is expected to play an important role in the structure and properties of CYPOR, which at present is unknown. To fill this gap in our knowledge and to investigate in greater detail the structure and role of the 140s loop in establishing the properties of rat CYPOR, we have deleted the two glycine residues one at a time (Gly-141 or Gly-143) in the "140s loop." The crystal structures of wild type and the three 140s loop mutant proteins in both the oxidized and reduced forms provide a molecular underpinning that accounts for the perturbed activity of the mutant proteins with their redox partners and the biochemical properties of the mutants.

Experimental Procedures

Materials—NADPH, sodium dithionite, FMN, dithiothreitol, Triton X-100, benzphetamine, horse heart cytochrome *c*, DEAE-Sepharose Fast Flow resin, and octyl-Sepharose CL-4B were purchased from Sigma. Potassium phosphate, glycerol, tryptone, sodium chloride, and yeast extract were purchased from Fisher. Hydroxyapatite and Bio-Beads were from Bio-Rad. The Complete Mini protease inhibitor mixture tablets and redistilled glycerol were purchased from Roche Diagnostics. The C41 (DE3) *Escherichia coli* cells were purchased from Avidis (France). Isopropyl β-D-thiogalactopyranoside and carbenicillin (disodium salt) were from Research Products International Corp. Dilauroylphosphatidylcholine was from Doosan Serdary Research Laboratory (Toronto, Canada). YM30 membrane was from Millipore (Billerica, MA). The Pierce BCA assay kit was purchased from Thermo Scientific (Rockford, IL).

TABLE 1
Sequences of oligonucleotide primers used to mutate full-length and truncated (57–678) CYPOR

Mutant	Sequence
ΔGly-141 (forward)	5′-TGC ATG GCC ACA TAC–GAG GGC GAC C-3′
ΔG141/E142N (forward)	5′-TGC ATG GCC ACA TAC–**AAC** GGC GAC C-′
ΔGly-143 (forward)	5′-ATG GCC ACA TAC GGA GAG–GAC CCC A-3′
Stop codon (forward)	5′-GCC ACT GGG GAG GAG **TAG TAG** ATT C-′

Site-directed Mutagenesis of the Full-length and Truncated Δ56 CYPOR (Residues 57–678)—The site-directed mutants of the full-length or soluble (residues 57–678) rat CYPOR were prepared by the PCR method using the QuikChange II XL site-directed mutagenesis kit (Agilent Technologies). The oligonucleotides used to generate the reductase mutants were designed according to the guidelines from the QuikChange II XL site-directed mutagenesis kit and were synthesized by Integrated DNA Technologies (Coralville, IA). Table 1 shows the oligonucleotides used to mutate full-length CYPOR. The mutated plasmids were extracted and purified using the QIAprep mini-kit (Qiagen, Chatsworth, CA). Following mutagenesis, the nucleotide sequence of the entire mutated reductase was determined at the University of Michigan DNA Sequencing Core Facility to confirm the presence of the desired mutation and the absence of any unwanted base changes.

The FMN domain-only mutants (residues 57–240) for the ΔGly-141, ΔG141/E142N, and ΔGly-143 mutants of the soluble truncated CYPOR(57–678) were prepared by the PCR method using the QuikChange II XL site-directed mutagenesis kit. Briefly, the oligonucleotides with two stop codons at positions Ser-240 and Ser-241 were generated according to the guidelines from QuikChange II XL site-directed mutagenesis kit and were purchased from Integrated DNA Technologies. The truncated ΔGly-141, ΔG141/E142N, and ΔGly-143 mutant plasmids were used as templates for the generation of the FMN domain-only mutants. The mutated plasmids were purified as described above, and the sequence of the entire plasmids was determined at the University of Michigan DNA Sequencing Core Facility.

Expression and Purification—Expression of the full-length (residues 1–678), truncated (57–678), and FMN domain only (57–240) CYPOR was performed in freshly transformed competent C41 (DE3) *E. coli* and grown in 1 liter of LB media containing 0.24 M carbenicillin, 0.2% (w/v) glucose, and 5.3 nM riboflavin. The full-length, truncated, and FMN domain wild type and mutants were purified as described previously in detail (37, 38). The mutant reductases could be purified by the same procedure as the corresponding wild type. The average yield of pure full-length mutants, wild type, and mutant reductase proteins was ~20–25 mg/liter. Significantly better expression and yield of pure protein (~100–150 mg/liter) were obtained with the truncated and FMN domain proteins. The amount of the diflavin protein was determined using $\epsilon_{454\,nm}$ = 21.4 mM^{-1} cm^{-1} and the Pierce BCA protein assay (Thermo Scientific, Rockford, IL). A molar extinction coefficient of 12.2 mM^{-1} cm^{-1} was used to determine the concentration of the FMN domain-only proteins. All the mutants and WT CPR ran as a single band on SDS-PAGE.

Determination of the Flavin Content of WT CYPOR and the Glycine Deletion Mutants—The FAD and FMN content in WT CYPOR and the glycine deletion mutants were determined using an HPLC method according to the published procedures (39). The HPLC assay was performed on a Beckman Coulter System Gold HPLC instrument connected to the JASCO FP-2020 Plus Intelligent Fluorescence Detector and a PC work station. The separation of both FAD and FMN was accomplished on a reverse-phase (4.6 × 250 mm) C18 column (LiChrospher 5RP18, Varian Inc.) with a mobile phase of 20% methanol, 80% 5 mM potassium phosphate buffer, pH 6.0 (v/v). Elution of both flavins was monitored at 268 nm, and the concentration of their standard solutions was determined using molar extinction coefficients of $\epsilon_{450\,nm}$ FMN = 12.2 mM^{-1} cm^{-1} and $\epsilon_{450\,nm}$ FAD = 11.3 mM^{-1} cm^{-1} (39). The total amount of mutant or WT reductase to be loaded to the HPLC instrument was determined by the Pierce BCA protein assay (Thermo Scientific, Rockford, IL).

Determination of CYPOR Activity Using Cytochrome c and Ferricyanide—The ability of the deletion mutants to reduce cytochrome *c* and ferricyanide was measured in 270 mM potassium phosphate buffer, pH 7.7, at 30 °C as described previously (37). Briefly, cytochrome *c* (65 μM final concentration) in 270 mM potassium phosphate buffer, pH 7.7, was incubated in a cuvette for 5 min at 30 °C. After 5 min, CYPOR was added to a final concentration of 9 nM to cyt *c*, and the reaction was immediately initiated by addition of NADPH (50 μM final concentration). The initial rate of cyt *c* reduction was followed for 5 min at 550 nm. The reduction of ferricyanide was measured at 30 °C in a solution containing 10 nM CYPOR with 500 μM ferricyanide (final concentrations of CYPOR and ferricyanide). The reaction was initiated by addition of NADPH to a final concentration of 100 μM. The initial rate of ferricyanide reduction was followed for 5 min at 420 nm. The rate of cyt *c* and ferricyanide reduction was determined using $\Delta\epsilon$ = 21.1 mM^{-1} cm^{-1} at 550 nm and 1.02 mM^{-1} cm^{-1} at 420 nm, respectively.

Measurement of Benzphetamine Metabolism by Cyt P450 2B4—Wild type cyt P450 2B4 was expressed and purified as described previously (37, 40). The metabolism of benzphetamine at 30 °C under steady-state conditions was determined by measuring formaldehyde formation using Nash's reagent according to the published procedures (37, 41).

Kinetics of the Reduction of CYPOR by NADPH—The kinetics of reduction of CYPOR by NADPH was carried out at 25 °C under anaerobic conditions using a Hi-Tech SF61DX2 stopped-flow spectrophotometer equipped with a temperature-controlled circulating water bath, housed in an anaerobic Belle Technology glove box (Hi-Tech, Salisbury, UK) as described previously (37). The buffer contained 100 mM potassium phosphate, pH 7.4, and 10% (v/v) glycerol.

Autoxidation of the Two-electron Reduced WT CYPOR and the Glycine Deletion Mutants—To characterize the autoxidation of WT CYPOR and the deletion variants, the two-electron reduced protein at 10 μM in 100 mM potassium phosphate buffer, pH 7.4, and 10% (v/v) glycerol was loaded into one syringe of a Hi-Tech stopped-flow apparatus in a glove box. The diflavin reductases were reduced with 1 molar eq of NADPH. The FMN domains were reduced by two-electron equivalents

by a standardized solution of dithionite. Oxygen-saturated buffer (100 mM potassium phosphate, pH 7.4, containing 10% glycerol (v/v)) was loaded into a second syringe. The final concentration of the reductases was 5.0 μM after mixing at 25 °C. The contents of the two syringes were rapidly mixed using the stopped-flow spectrophotometer, and the absorbance changes occurring during autoxidation of the reductases were recorded in the single wavelength mode between 452 and 466 nm and 590 nm. The absorbance was followed at the absorbance maxima of the different proteins.

Anaerobic Reduction of WT CYPOR and the Mutant Reductases with Sodium Dithionite—The reduction of WT CYPOR and the glycine deletion mutants with a standardized solution of sodium dithionite was carried out in a tonometer connected to a gas-tight Hamilton syringe that was assembled in an anaerobic Belle Technology glove box (Hi-Tech, Salisbury, UK). All the UV-visible absorbance spectra were recorded on a Cary 300 spectrophotometer in a tonometer outside of the glove box (Varian Inc.) at 25 °C in 100 mM potassium phosphate buffer, pH 7.4. Prior to introduction into the glovebox, the buffer containing ~20 μM WT reductase or mutant was purged with nitrogen and placed inside the glove box overnight at 4 °C. The titrant (sodium dithionite) was prepared inside the glove box and standardized with a solution of ferric cytochrome b_5 (41). Before titration of the reductases, a small amount of mediator, methyl viologen (~0.5 μM), was added to the protein (20 μM final concentration). The redox titrations were performed as described previously (42). Specifically, a small aliquot of sodium dithionite was added to the dye/protein buffer mixture, and the solution was mixed thoroughly and allowed to reach equilibration (~10–15 min), and then the spectrum was recorded using a Cary 300 UV-visible spectrophotometer. The titration was continued until a four-electron reduced enzyme was formed.

Determination of the Midpoint Potentials of the WT and Mutant Diflavin and FMN Domains—All redox titrations were performed in an anaerobic glove box (Belle Technology, Weymouth, UK) under N_2 atmosphere with less than 2 ppm oxygen levels. Absorption spectra were recorded with a Cary 50 spectrophotometer using a dip probe detector, and the potentials were determined using a Accumet AB15 coupled to a silver/silver chloride electrode saturated with 4 M KCl. Measurements were done in a custom-made glass beaker kept in a water bath at 15 ± 1 °C. The reductive titration was performed by stepwise addition of small aliquots of sodium dithionite (42). Potentials recorded against the silver/silver chloride reference electrode were converted to values *versus* the standard hydrogen electrode using a conversion factor of +214 mV at 15 °C. The concentration of all the reductases was ~40 μM. All protein samples were first oxidized with ferricyanide. The oxidized protein was then separated from the excess ferricyanide and ferrocyanide by size exclusion chromatography using a cyanide Sephadex G-25 column (PD-10, GE Healthcare). All measurements were performed in 100 mM potassium phosphate buffer, pH 7.4, with 10% glycerol (v/v). The redox mediators used (~3 μM final concentration) with their midpoint potentials *versus* a standard hydrogen electrode are as follows: phenazine metasulfate (+80 mV), 2-hydroxy-1,4-naphthaquinone (−152 mV), anthroquinone-2-sulfonate (−225 mV), phenosafranine (−252 mV), benzyl viologen (−374 mV), and methyl viologen (−443 mV). Prior to and after use in redox titrations, the potential response of the ORP microelectrode was checked against a saturated quinhydrone solution in 100 mM phosphate, pH 7.0 (+301 mV at 22 °C), as well as in a solution of 5 mM ferricyanide/ferrocyanide redox couple in 100 mM phosphate, pH 7.0, (+425 mV at 22 °C). The response of the electrode was in good agreement with listed values for the redox couples used (within ±5 mV). Absorbance changes between 380 and 390, 585, and 454 and 469 nm maxima for the red semiquinone, blue semiquinone, and oxidized flavins, respectively, were plotted against the measured potentials at each point of the titration. The absorbance was plotted at 375 and 454 nm for the E142N mutant. Midpoint potentials for both the oxidized/semiquinone and semiquinone/hydroquinone couples of the FMN domains were estimated by fitting the plot of the midpoint potentials to Equation 1, which was derived from the Nernst equation and Beer-Lambert law according to the published procedures (29, 43).

$$A = \frac{a \times 10^{(E-E1)/59} + b + c \times 10^{(E2-E)/59}}{1 + 10^{(E-E1)/59} + 10^{(E2-E)/59}} \quad \text{(Eq. 1)}$$

Equation 1 is for a two-electron redox process, where *a*, *b*, and *c* are the relative absorbance values of the oxidized, semiquinone, and hydroquinone forms of flavin, respectively. *A* is the total absorbance. *E* is the potential at the working electrode, and E_1 and E_2 are the midpoint potentials of the ox/sq and sq/hq redox couples. The five variables were determined by least squares fitting.

In the diflavin wild type CYPOR, the midpoint potentials were obtained for both the FMN and FAD domains. The data were fit to Equation 2, which represents the sum of two two-electron redox reactions as described previously (29).

All data manipulation and non-linear least squares curve fitting were performed using OriginLab (version 8.6, Northampton, MA). For WT CYPOR, the absorbance at 380, 454, and 585 nm was plotted as a function of the system potential at each point in the titration when equilibrium had been reached. The absorbance at 380, 459, and 592 nm was plotted against the system potential for the ΔGly-143 mutant. The absorbance at 388 and 468 nm was plotted against the system potential for the ΔGly-141 mutants because the absorbance of the blue semiquinone was undetectable.

$$A = \frac{a10^{(E-E'1)/59} + b + c10^{(E'2-E)/59}}{1 + 10^{(E-E'1)/59} + 10^{(E'2-E)/59}} + \frac{d10^{(E-E'3)/59} + e + f10^{(E'4-E)/59}}{1 + 10^{(E-E'3)/59} + 10^{(E'4-E)/59}} \quad \text{(Eq. 2)}$$

In Equation 2, *A* is the total absorbance; *a, b,* and *c* are the absorbance values contributed by one flavin in the oxidized, semiquinone, and hydroquinone states, respectively; and *d, e,* and *f* are the corresponding absorbance components associated with the second flavin. *E* is the observed potential; $E'1$ and $E'2$ are the midpoint potentials for oxidized/semiquinone and semiquinone/hydroquinone couples, respectively, for the first flavin, and $E'3$ and $E'4$ are the corresponding midpoint potentials for the second flavin.

TABLE 2
Data collection and refinement statistics

	Wild type[a]		ΔGly-141		ΔG141/E142N		ΔGly-143	
Protein	Oxidized	Reduced	Oxidized	Reduced	Oxidized	Reduced	Oxidized	Reduced
PDB codes	4YAF	4YAL	4Y9R	4YAW	4Y7C	4YAU	4Y9U	4YAO
Resolution, Å	50–1.91	50–1.88	50–2.4	50–2.0	50–2.2	50–2.2	50–1.95	50–2.5
No. of total references	1,287,618	1,283,330	554,662	700,411	526,475	270,308	483,860	215,783
No. of unique references	107,981	113,658	56,024	95,227	71,520	68,638	98,601	45,775
Completeness (%)	99.8 (99.8)[b]	99.9 (100)	99.9 (99.8)	91.6 (100)	99.6 (96.3)	95.1 (72.7)	95.3 (67.0)	94.8 (95.6)
Redundancy	11.9 (11.7)	11.3 (11.1)	9.9(9.2)	7.4(6.3)	7.4(5.5)	4.0(3.5)	4.9(3.2)	4.8(4.2)
$I/\sigma(I)$	38(4.1)	38(4.0)	32(3.4)	34(3.2)	26(3.0)	27(2.6)	23(2.2)	23(2.7)
R_{symm}	0.067 (0.681)	0.067 (0.666)	0.074 (0.658)	0.055 (0.618)	0.076 (0.550)	0.045 (0.448)	0.059 (0.539)	0.064 (0.640)
Space group	$P\,2_12_12_1$	$P\,2_12_12_1$	$P\,2_12_12_1$	$P\,2_12_12_1$	$P\,2_12_12_1$	$P\,2_12_12_1$	$P\,2_12_12_1$	$P\,2_12_12_1$
Unit cell *a, b, c,* Å	102.0, 115.3, 118.9	101.8, 115.4, 118.3	102.0, 115.9, 119.7	101.5, 116.0, 118.5	101.5, 115.6, 118.9	101.6, 115.9, 118.6	101.8, 115.1, 119.5	101.5, 115.5, 117.6
Refinement								
Resolution range (Å)	50–1.91	50–1.88	50–2.4	50–2.0	50–2.2	50–2.2	50–1.95	50–2.5
$R_{crystal}$	0.205	0.196	0.195	0.204	0.192	0.201	0.203	0.234
R_{free}	0.239	0.228	0.254	0.252	0.244	0.241	0.241	0.298
No. of water molecules	1106	1225	649	1178	1138	684	1083	291
Ramachandran analysis (%)								
Most favored	97.3	97.9	96.8	97.3	97.0	95.9	97.5	93.1
Allowed	2.5	1.9	3	2.6	2.8	3.9	2.3	6.8
Generously allowed	0.2	0.2	0.2	0.2	0.2	0.2	0.2	0.2
Disallowed	0	0	0	0	0	0	0	0
***B*-factor analysis, Å^2**								
Molecule A, all atoms	34	28	42	34	29	44	34	54
Molecule A, 140s loop	50	35	58	59	39	50	70	73
Molecule B, all atoms	42	37	51	45	44	56	42	63
Molecule B, 140s loop	67	43	72	60	76	88	83	102

[a] Data for wild type crystals were collected at SBC 19ID, Advanced Photon Source, Argonne National Laboratory. All mutant data were obtained using an in-house Rigaku MicroMax-007/R-AXIS IV^{2+} system.
[b] Values in the parentheses are those for the highest resolution shell.

Crystallization and Data Collection—Prior to all crystallization setups, truncated, soluble (Δ56), and purified CYPOR proteins were dialyzed in 50 mM HEPES, pH 7.5, buffer and concentrated to a final concentration of ~15 mg/ml (~0.2 mM). Exogenous FMN (0.1-fold stoichiometric amount of the enzyme amount), 2 mM 2′-AMP, and 1 mM tris(2-carboxyethyl)phosphine were added to the final protein sample. Crystals were grown using the hanging drop method (44) by mixing 5 μl of the protein solution and 2 μl of reservoir solution (150 mM HEPES, pH 7.0, 150 mM sodium acetate, and 20% (w/v) PEG 4000). Diffraction quality crystals were obtained within 7–10 days at 19 °C. Freshly grown crystals were first transferred to a well solution containing 25% (w/v) PEG 4000 (cryosolution 1) and then transferred to another well solution with 30% (w/v) PEG 4000 (cryosolution 2), prior to flash freezing in liquid nitrogen. Diffraction data for all mutants were collected using an in-house facility (Rigaku MicroMax-007/R-AXIS IV^{++} system). Data sets for the wild type enzyme were collected at the Structural Biology Center Beamline 19-ID, Advanced Photon Source, Argonne National Laboratory (Argonne, IL). All data sets were processed and scaled using HKL2000 (45). Reduced protein crystals were obtained by soaking preformed crystals of oxidized protein in cryosolution 2 plus 50 mM sodium dithionite at room temperature, until the crystal became completely colorless (~5 min). Then the crystal was immediately flash frozen by dipping into liquid nitrogen.

Structure Determination—Initial phases were calculated from the published high resolution structure of a rat CYPOR mutant (Protein Data Bank accession code, 1JA1) (27). Multiple rounds of reciprocal space refinement were carried out using CNS 1.3 (46), and subsequent manual fitting with the program COOT (47) was performed using $(2|F_o| - |F_c|)$ and $(|F_o| - |F_c|)$ maps. Water molecules were assigned when densities greater than 3σ were observed in the $|F_o| - |F_c|$ map that were within at least 3.3 Å of a potential hydrogen-bonding partner. Data collection and the refinement statistics are given in Table 2.

TABLE 3
Amino acid sequence alignment for the FMN binding loop of the diflavin reductase family and two flavodoxins
The conserved glycine colored red is absent in BM3. The other conserved glycine is colored green.

Cytochrome P450 Reductase	139 **TYGEGDPTD** 147
P450 BM3 Reductase	536 **SY-NGHPPD** 143
Neuronal Nitric Oxide Synthase (nNOS)	808 **TFGNGDPPE** 816
Sulfite Reductase	117 **TQGEGEPPE** 125
Methionine Synthase Reductase	59 **TTGTGDPPD** 67
Clostridium beijerinckii flavodoxin	55 **AMGDEVLEE** 63
Desulfovibrio vulgaris flavodoxin*	59 **TWGDDSIELQD** 69

* *D. vulgaris* has a longer loop.

Results

Rationale for the Mutations in the "140s Loop," Residues 140YGEGD144

To gain insight into how the environment of the flavin in flavoproteins controls the redox state and reactivity of the FMN of CYPOR, we deleted either Gly-141 or Gly-143, both of which are located in the 5-amino acid loop between β-strand 3 at the amino terminus of the loop and α-helix 5 at its carboxyl terminus. In flavodoxins, whose potentials can differ by as much as 400 mV and in other members of the diflavin oxidoreductase family, these residues have been shown to be important determinants of both oxidized/semiquinone and semiquinone/hydroquinone redox couples (24, 29, 33, 43). Sequence alignment of the FMN binding loop of the diflavin reductase family and two flavodoxins (Table 3) reveals that Gly-143 is conserved in all members of the diflavin reductase family, but it is not con-

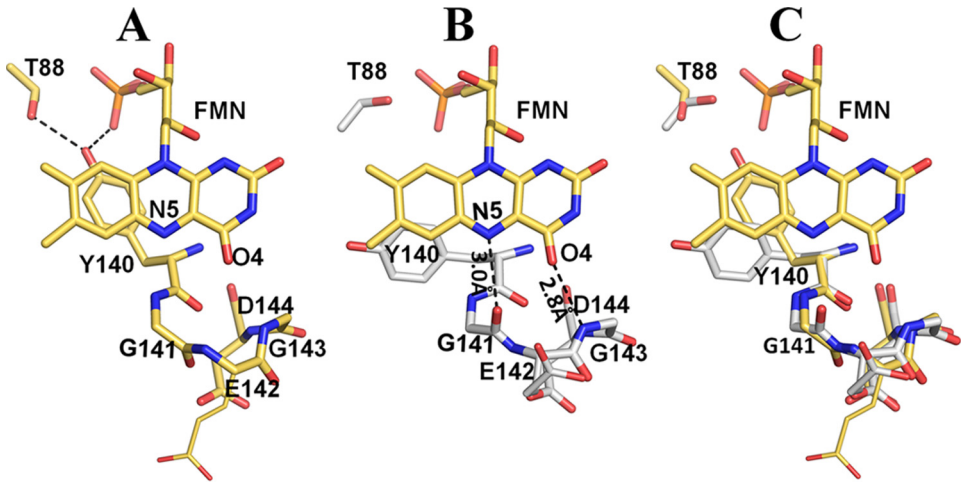

FIGURE 1. **Structures of wild type CYPOR in the vicinity of the FMN isoalloxazine ring, in the oxidized state (*A*), reduced state (*B*), and a superposition of oxidized and reduced structures (*C*).** In the oxidized structure, the five-membered 140s loop forms a double β-turn with the Gly-141–Glu-142 peptide bond adopting an O-down conformation. When the crystalline protein was reduced, the peptide bond flips to form an O-up conformation. Superposition of oxidized and reduced structures clearly shows the peptide bond isomerization (*C*), resulting in the formation of two H-bonds from N5 and O4 atoms of the flavin ring to the Gly-141 carbonyl oxygen and the amide nitrogen of Gly-143, respectively. These H-bonds stabilize the loop conformation, which in turn stabilizes the FMN semiquinone. In addition, when the protein is reduced, the phenolic side chain of Tyr-140 swings out from the *re*-face of the isoalloxazine ring, resulting in the loss of two hydrogen bonds (Tyr-140 hydroxyl to both Thr-88 and FMN phosphate oxygen). Of the two molecules in the asymmetric unit, the structure of molecule A is used for all figures, because it is better ordered than molecule B (see average *B*-factors in Table 2). Figs. 1–5 were generated using PyMOL Molecular Graphics System, version 1.2r3pre. Schrödinger, LLC (DeLano Scientific). Corresponding electron density map for each figure (Figs. 1–4) are included in the supplemental material.

served in some flavodoxins. To our knowledge, the role of Gly-143 in determining the properties of diflavin reductase has not been previously investigated. Gly-141, however, is conserved in many flavodoxins and in the entire diflavin reductase family except in the cyt P450 BM3 reductase (23, 34). The ΔGly-143 mutant was constructed to gain insight into how a loop shortened at a position downstream from the Gly-141 and therefore with a different sequence and structure might perturb the function of the 140s loop. The double mutant ΔG141/E142N, whose sequence is identical to that of the cyt P450 BM3 reductase domain, and ΔGly-141 were constructed to investigate the effect of shortening the loop at position 141 *versus* 143 and to observe whether the amino acid at position 142 was functionally important in CYPOR. Thus, the three deletion mutants, namely ΔGly-143, ΔGly-141, and ΔG141/E142N, were expressed, purified, and characterized. Because of lack of a side chain, glycine residues can assume a wider range of backbone torsion angles than any other amino acid and thus may play a crucial role in controlling the 140s loop flexibility and conformation, which in turn would regulate the FMN redox properties and function of the reductase. Thus, shortening the loop by deleting either Gly-141 or Gly-143 may interfere with the ability of CYPOR to regulate the properties of the reduced FMN.

Crystal Structures of the Wild Type and Glycine Deletion Mutants

All CYPOR crystals studied here are isomorphous (Table 2), and there are two molecules in the asymmetric unit, molecule A and molecule B. Because molecule A is better ordered than molecule B (see *B*-factor values in Table 2), the following structural results are based on molecule A, unless noted otherwise.

Wild Type Structures

Because the previously reported structure of wild type CYPOR (26) is of a relatively low resolution (2.6 Å; PDB code, 1AMO) and because we are interested in the exact conformations of the 140s loop in both the oxidized and reduced states, we set out to determine a higher resolution structure (1.9 Å) of the wild type using crystals that were obtained under the same conditions as the mutant crystals. As expected, the overall fold of the current, 1.9 Å wild type structure (Fig. 1 and supplemental Fig. S1), is the same as other CYPOR structures that have been published previously, including structures of wild type (1AMO (26)) and various mutants of rat (27, 48), and human CYPORs (28). However, despite the relatively higher resolution, the 140s loop in the current oxidized structure is still more disordered and flexible compared with other parts of the polypeptide (*B*-factors 50 A^2 *versus* 34 A^2 in molecule A). The 140s loop is also more disordered in other previously determined CYPOR structures, most likely due to the presence of the two glycines in the loop (26, 27). In the current relatively high resolution oxidized structure, the five-residue loop forms a double β-turn (49) and the Gly-141 carbonyl oxygen of the Gly-141–Glu-142 peptide bond adopts an "O-down" conformation that points down and away from the flavin ring (Fig. 1), similar to the structure of human CYPOR (28). In some of our earlier published rat CYPOR wild type and mutant structures (PDB codes 1AMO, 1JA1, 1JA0, and 1J9Z) (26, 27), the Gly-141– Glu-142 peptide conformation was modeled with an O-up conformation as in a type II′ turn that forms an H-bond between the Gly-141 carbonyl and the FMN N5 atom similar to that seen in the reduced flavodoxin structure (34), possibly due to a lower resolution. It is also possible that the crystalline proteins reported by Wang *et al.* (26) were partially reduced by the x-ray irradiation during data collection. This may also be true with some flavodoxin structures, as both the O-down and O-up conformations have also been observed for both the oxidized and blue neutral semiquinone in *Clostridium beijerinckii* flavodoxins (34), *Desulfovibrio vulgaris* (35), and *Aspergillus nidulans*

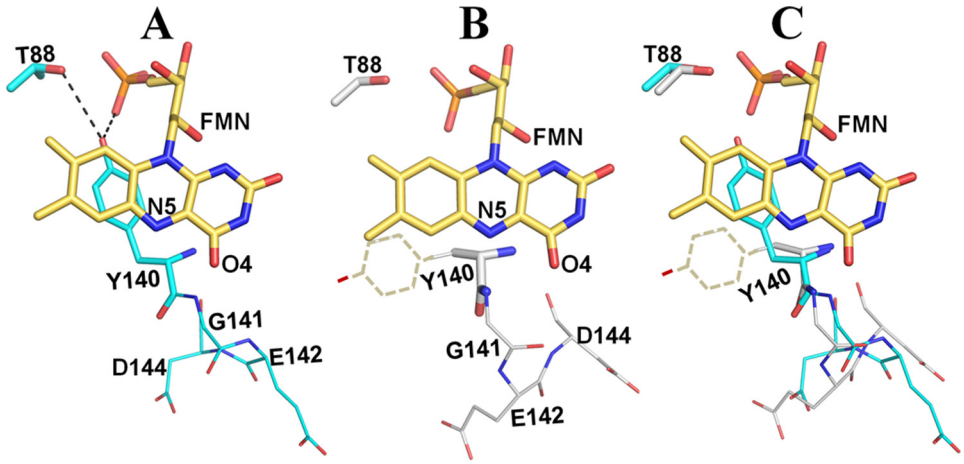

FIGURE 2. **Structures of ΔGly-143 CYPOR in the vicinity of the FMN ring, in the oxidized state (*A*) and reduced state (*B*), and a superposition of both structures (*C*).** The 140s loop in this mutant is one residue shorter than that of wild type. The loop structure is extremely mobile (see supplemental Fig. S2 for electron density map). The average *B*-factor for the Tyr-140–Asp-144 (wild type residue numbering) loop is 69.9 Å^2 (for molecule A) compared with the average *B*-factor of 33.6 Å^2 for the entire molecule A. The disordered part of the loop is represented by *thin sticks*. There is no H-bond between the flavin ring and the loop. However, as in the wild type structures, there are two H-bonds from the Tyr-140 hydroxyl group to both Thr-88 and a phosphate oxygen of FMN. In the reduced structure, only the main chain atoms of Tyr-140–Gly-141of the entire 140s loop can be clearly modeled, and the rest of the loop structure shown with *thin sticks* represents a possible modeled structure. Furthermore, the phenol ring of Tyr-140 is completely disordered, and a possible location of the ring is shown with *dotted lines* (see supplemental Fig. S2 for the electron density map).

(50). However, our more recent higher resolution structures of human (PDB codes 3QE2, 3QFC, and 3QFR) (28) and rat mutant CYPOR (PDB codes 3OJX and 3OJW) (48), which were crystallized under different conditions, with extra precautions to avoid protein reduction during data collection, show that the Gly-141 carbonyl group adopts an O-down conformation similar to that observed in the oxidized *C. beijerinckii* flavodoxin structure. However, there was still a hint of the presence of the O-up conformation, suggesting that a very minor portion of the crystalline protein had been reduced during the data collection. In some oxidized human CYPOR structures, a water molecule bridges the FMN N5 and the Glu-142 main chain amide nitrogen (28).

In the O-down conformation observed in the structures of the fully oxidized form of both wild type CYPOR and flavodoxins, little interaction between the Gly-141 loop residues and the FMN ring was observed (Fig. 1*A*). However, when the crystals of the wild type protein were reduced with dithionite presumably to a fully reduced hydroquinone state or a mixture of the stable blue semiquinone and hydroquinone (because the crystals were almost completely colorless), the Gly-141 carbonyl group adopts a clear O-up conformation (Fig. 1*B*), as observed in the reduced forms (both semiquinone and hydroquinone) of flavodoxin from *C. beijerinckii* (34) and in the semiquinone form of rat nNOS reductase domain (32). Supplemental video 1 shows a plausible 140s loop movement from the O-down to O-up conformation. The reduced wild type CYPOR structure showed two H-bonds between the flavin and 140s loop residues: one between N5H of the FMN hydroquinone and the Gly-141 carbonyl oxygen and the other between O4 of FMN and the main chain amide nitrogen of Gly-143.

In the oxidized structure, the OH of the phenolic ring of Tyr-140, which stacks at a 30° angle with the FMN ring, makes two H-bonds, one with a phosphate oxygen of FMN and the other with the side chain OH of Thr-88. Interestingly, in the reduced structure, the phenolic ring of Tyr-140 has rotated. This rotation of the Tyr-140 ring results in the loss of two H-bonds, one to the phosphate of FMN and the second to the Thr-88 side chain. Thus, the conformational change upon reduction of the oxidized flavin results in the loss of two H-bonds but the gain of two new H-bonds between the reduced flavin and the backbone atoms of the 140s loop. Although we do not have the structure of the blue semiquinone form of CYPOR, it is most likely that the blue semiquinone structure would be the same as that of the hydroquinone form, as it is in the case of flavodoxins (34, 35, 51). In addition, the structure of the air-stable blue semiquinone form of nNOS reductase domain also has the O-up conformation (32). The two H-bonds formed between the FMN ring and the 140s loop and the conversion from the O-down to the O-up conformations between the oxidized and reduced forms are important factors defining the FMN redox potentials, stability of the neutral blue semiquinone, and the redox state of CYPOR capable of the electron transfer to its redox partners (10). Tuning the relative strength of the hydrogen bonds between the flavin and polypeptide provides a mechanism by which the protein environment alters the reactivity of the flavin (34).

Crystal Structures of Oxidized and Reduced ΔGly-143

Gly-143 is conserved in all known diflavin reductase family members and some flavodoxins (Table 3) (52). In the ΔGly-143 mutant, the wild type 5-residue 140s loop has been shortened by one residue, resulting in a turn with the sequence ^{140}YGED^{144} (the wild type residue numbering). Amazingly, the entire shortened 140s loop (Tyr-140–Pro-145) conformation is poorly defined with high average *B*-factors (>70 Å^2) in both oxidized and reduced structures compared with the rest of the molecule (34 Å^2 for the oxidized and 54 Å^2 for the reduced form) (Fig. 2 and supplemental Fig. S2). As in the oxidized structures of the WT, the hydroxyl group of the Tyr-140 side chain in the oxidized ΔGly-143 structure is H-bonded to a phosphate oxygen of FMN and the side chain of Thr-88. How-

ever, in the reduced structure the Tyr-140 phenolic side chain is highly disordered. As a result, H-bonds between Tyr-140 and phosphate oxygen and Thr-88 side chain could not be found, indicating that these H-bonds are lacking or markedly weakened (Fig. 2). Furthermore, the ΔGly-143 mutant is unique compared with the WT and ΔGly-141 mutants. There is no H-bond between N5H of the flavin and the ΔGly-143 polypeptide backbone in both the oxidized and reduced structures. Nevertheless, in solution, it is likely that the reduced flavin is protonated and the N5H acts as an H-bond donor and forms a weak (transient) H-bond directly with the disordered loop or via a solvent molecule. As will be discussed below, a small amount of an unstable blue semiquinone is formed under anaerobic conditions when the separate FMN domain is reduced, indicating that the loop forms an H-bond with the protonated flavin N5. Free reduced flavin in aqueous solution does not form a stable H-bond with water.

The sequence of a four-residue turn with a tyrosine and a glycine in the i and $i + 1$ key positions, respectively, as in the case of ΔGly-143 generally favors a type II′ turn (49). In the ΔGly-143 structure, however, formation of a type II′ turn would result in a steric collision between the Gly-141 carbonyl oxygen and the O4 of the FMN. To minimize the steric collision, the entire loop in the ΔGly-143 structure forms a highly *disordered* loop structure. This steric collision may also account for the decreased affinity of the flavin for the ΔGly-143 protein. Interestingly, the purified protein contains only 78% of the expected amount of FMN (Table 4). This lower affinity of oxidized ΔGly-143 for FMN is unlikely due to the lack of stable H-bonds between N5 and O4 of FMN and the 140s loop residues, because no such H-bonds exist in the oxidized WT. Instead, it is most likely due to the steric hindrance between the FMN isoalloxazine ring and the Gly-141 loop, if a standard type II′ β-turn were formed.

TABLE 4
Flavin content of wild-type and mutant CYPOR

CYPOR reductase mutant/WT	FAD content	FMN content
	pmol/pmol protein	*pmol/pmol protein*
WT CYPOR	96 ± 0.2	92 ± 0.5
ΔGly-141	98 ± 0.1	93 ± 0.3
ΔG141/E142N	98 ± 0.2	91 ± 0.2
ΔGly-143	97 ± 1.0	78 ± 0.5

In the reduced ΔGly-143 structure, electron density for the 140s loop is observed only for backbone atoms of Tyr-140 and not for the side chain of Tyr-140. There are some densities for the rest of the 140s loop (supplemental Fig. S2). However, no definitive conformation can be modeled in, which is an additional indication that the loop is highly disordered. A low affinity for FMN was also observed in the N537G/G538A double mutant of P450 BM3 reductase domain (mutant loop sequence YGAH) on the corresponding loop of the FMN domain. However, as in the ΔGly-143 mutant, the Gly-537 in the $i + 1$ corner position of the loop in the double mutant would result in a preference for a type II′ turn, which would cause steric hindrance with FMN resulting in a 10-fold higher K_d value (*i.e.* lower affinity) for FMN in the P450 BM3 protein compared with the wild type (36). Unfortunately a structure of the corresponding BM3 reductase mutant is not available.

Crystal Structures of Oxidized and Reduced ΔGly-141 and ΔG141/E142N

Oxidized Structures—The structures of the Gly-141 deletion mutants, ΔGly-141 (Fig. 3 and supplemental Fig. S3) and ΔG141/E142N (Fig. 4 and supplemental Fig. S4), are very similar, except that the side chain of Glu-142 (wild type numbering) is disordered and appears to have two conformations (Fig. 3*A*) in the ΔGly-141 structure, whereas the Asn-142 side chain is well ordered in the double mutant, ΔG141/E142N. As in the ΔGly-143 mutant, the 140s loop in both mutants is one residue shorter than that of wild type, resulting in a tighter loop that places the peptide bond of Glu-142–Gly-143 much closer to the FMN ring. In addition, the four residues ^{140}YEGD^{144} (or YNGD

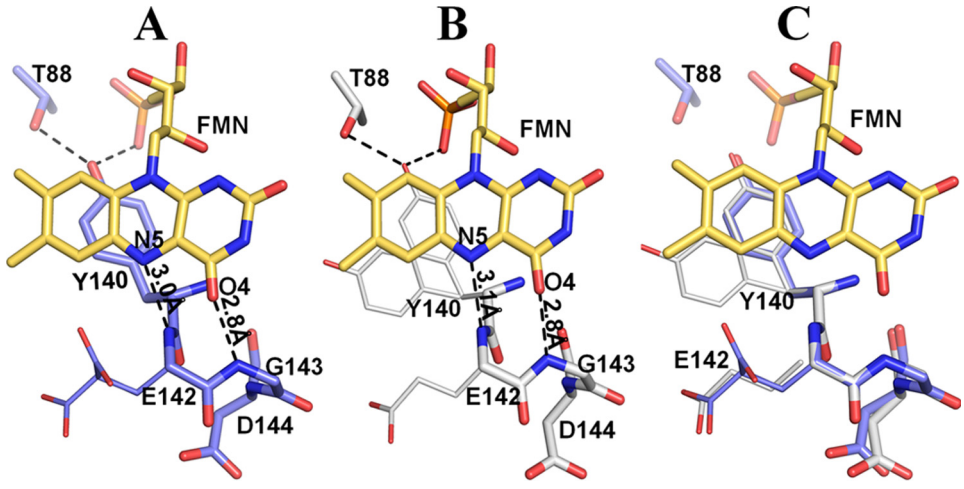

FIGURE 3. **Structures of ΔGly-141 CYPOR in the vicinity of the FMN ring, in the oxidized state (*A*), reduced state (*B*), and a superposition of both structures (*C*).** The 140s loop is again one residue shorter than that of wild type. This shorter loop is now closer to the FMN ring and forms a typical type I′ β-turn with the main chain carbonyl oxygen of Tyr-140 pointing down away from the FMN ring. This results in the main chain amide nitrogens of Glu-142 and Gly-143 (wild type numbering) making two H-bonds with N5 and O4 of the FMN ring, respectively. However, the γ-carboxylate of E142 adopts two conformations (shown in *thin sticks*), one of which is close to the FMN N5 atom (~3.5 Å). The structure of the reduced form is essentially the same as the oxidized state, except that the Tyr-140 has two conformations. However, the γ-carboxylate of Glu-142 has now only one conformation pointing away from FMN, suggesting that the carboxylate in the alternative conformation observed in the oxidized structure would be too close to the protonated N5 of the reduced FMN.

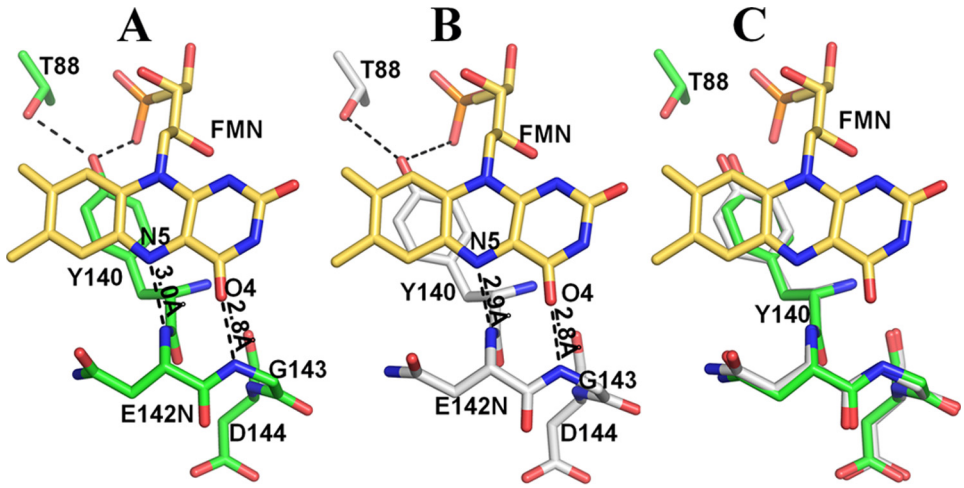

FIGURE 4. **Structures of ΔG141/E142N CYPOR in the vicinity of the FMN ring, in the oxidized form (*A*), reduced form (*B*), and a superposition of both structures (*C*).** Both oxidized and reduced structures are almost identical, and they are also very similar to those of ΔGly-141, except that the Asn-142 side chain is clearly defined in the double mutant structure. As in the wild type structure, the Tyr-140 hydroxyl group makes two H-bonds with the Thr-88 and a phosphate oxygen of FMN. Furthermore, as in the ΔGly-141 structures, the two H-bonds between the flavin ring and the 140s loop (N5 and O4 of the flavin ring to the main chain amide nitrogen atoms of Asn-142 and Gly-143, respectively) are conserved in both oxidized and reduced structures.

in the double mutant) now form a rigid type I′ β-turn structure (49). In both mutant structures, two H-bonds are formed between the flavin isoalloxazine ring and the shortened 140s loop; they are between the main chain amide nitrogen of Glu-142 (or Asn-142) and N5, and the amide of Gly-143 and O4 of FMN (Figs. 3*A* and 4*A*). As in the oxidized structures of wild type and the Δ143 mutant, the oxidized ΔGly-141 and ΔG141/E142N structures, the hydroxyl group of the Tyr-140 side chain makes two H-bonds, one with the side chain of Thr-88 and another with the phosphate oxygen of FMN (Figs. 3*A* and 4*A* and supplemental Figs. S3*A* and S4*A*). The rigid type I′ β-turn structure observed in this loop region and its interactions with FMN are very similar to those observed in the oxidized structure of the heme- and FMN-binding domains of P450BM-3 (Fig. 5) (24). Therefore, biochemical properties of these mutants, including redox potentials and their thermodynamic reactivity, are expected to resemble those of the P450 BM3 reductase domain.

The additional mutation, E142N, in the double mutant does not produce a significant structural disturbance, except that the E142N mutation markedly decreases the mobility of the resulting type I′ β-turn. In fact, the structure of this loop region in ΔG141/E142N is better defined, and its average temperature factor is only moderately higher than the rest of the molecule (39 Å^2 *versus* 29 Å^2; resolution, 2.2 Å), although in the single mutant, ΔGly-141, the average temperature factor in the loop is much higher than the rest of the molecule (58 Å^2 *versus* 42 Å^2; resolution, 2.4 Å). Furthermore, the substituted residue, Asn-142, is better ordered than the corresponding Glu-142 in the single deletion mutant (Figs. 4*A* and supplemental Fig. S4A). It has been shown that Asn is one of the most favored residues at the $i + 1$ corner position of a type 1′ β-turn, whereas Glu is much less favored (49). The $i + 1$ position in a type I′ turn requires a φ angle close to +60°, and aside from glycine, asparagine, and to a lesser extent aspartate it is the amino acid most preferred in this position because it can occupy the left-handed α-helical region of the Ramachandran plot (49, 53). It has been

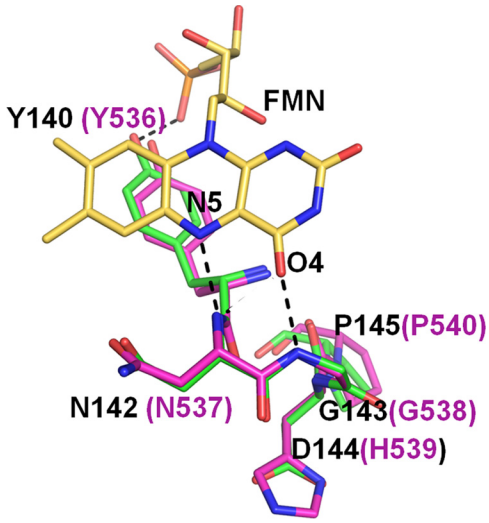

FIGURE 5. **Superposition of the structures of the 140s loops of ΔG141/E142N CYPOR (*green* carbon atoms) and P450 BM3 (*purple* carbons and lettering).** Both structures are in the oxidized state. Hydrogen bonds between the flavin ring and the amide nitrogen atoms of the loop are shown with *dashed lines*. Both structures are very similar, even though the loop sequences are slightly different (YNGDPT *versus* YNGHPP).

suggested that this increased type I′ turn stability is due to the ability of Asn and Asp to form a noncovalent attractive interaction between pairs of C(δ$^+$)=O(δ$^-$) carbonyl dipoles (53). A review of protein structures in the Protein Data Bank with a resolution better than 1.5 Å reveals that the Asn and Asp side chain carbonyls are observed to be within 4 Å of either their own backbone carbonyls or the backbone of the carbonyl of the previous residue ~80% of the time and the angle between the bond is ~90°. Although the resolution is rather low (2.03 Å), in the structure of the heme and FMN domains of P450 BM3, the side chain carbonyl of Asn-537 O(δ−) is ~4 Å from the carbon C(δ+) of the carbonyl group of Tyr-536. The low resolution (2.0–2.2 Å) of our ΔGly-141 mutant structures does not allow us to discern whether such an interaction occurs in the ΔGly-141 mutants. Thus, the fact that the loop structure in the double

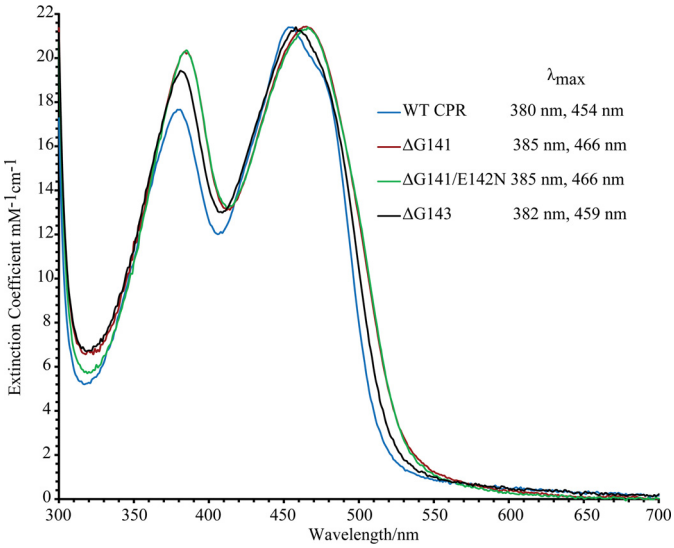

FIGURE 6. **UV-visible spectra of oxidized wild type and glycine deletion mutants of CYPOR.**

mutant is more stable is consistent with the notion that differences in turn stability arise mainly from interactions between the two central residues of a turn (*i.e.* $i + 1$ and $i + 2$ residues) (54). In the oxidized ΔGly-141 structure, the longer side chain of Glu-142 is disordered, but there is a hint of two conformations for the γ-carboxylate. Both conformations have very weak density. One conformation is closer to the FMN ring in the oxidized form (~3 Å to the C6 and N5 of the flavin ring).

Reduced Structures—The reduced structures of both ΔGly-141 (Fig. 3) and ΔG141/E142N (Fig. 4) are essentially the same as their corresponding oxidized structures except that in the reduced ΔGly-141 structure, the Tyr-140 side chain is disordered and appears to have two conformations, and although the carboxylate side chain of Glu-142 is disordered, there is no hint of the Glu side chain being close to the flavin (supplemental Fig. S3).

UV-visible Spectra of Oxidized WT CYPOR and the Glycine Deletion Mutants

The UV-visible spectrum of oxidized WT CYPOR (Fig. 6) is characterized by two peaks with absorbance maxima appearing at 380 nm ($\epsilon \cong 17\ mM^{-1}\ cm^{-1}$) and 454 nm ($\epsilon \cong 21.3\ mM^{-1}\ cm^{-1}$) and a shoulder at 479 nm, which is absent in the three mutant spectra. Both the 380- and 454-nm peaks have been assigned to π to π^* transitions (55). In all three mutants, the spectrum is red-shifted. The glycine deletion mutant designated as ΔGly-141 (Fig. 6) has its absorbance maxima red-shifted from 380 and 454 nm in WT CYPOR to 385 and 466 nm, respectively, in the mutant. A noticeable increase has also occurred in the intensity of the absorbance at 385 nm ($\epsilon \cong 20.5\ mM^{-1}cm^{-1}$ in ΔGly-141 *versus* $17\ mM^{-1}\ cm^{-1}$ in the wild type). However the absorbance intensity at 454 and 466 nm is similar in the wild type and mutant. These red shifts and changes in intensity of the 385-nm peak reflect the different polarity and chemical environment for the FMN isoalloxazine ring in the mutants compared with the wild type CYPOR (55, 56). The ΔG141/E142N mutant shows absorbance intensities and maxima that are red-shifted to the same extent as ΔGly-141.

In contrast, the absorbance maxima for the ΔGly-143 mutant are red-shifted by only 2 and 5 nm, respectively (to 382 and 459 nm), as compared with WT CYPOR. Although the intensity of the 454–466-nm peaks is similar in all three mutants and the wild type, the intensity of the absorbance of ΔGly-143 at 382 nm ($\epsilon \cong 19.3\ mM^{-1}\ cm^{-1}$) is intermediate between that of the wild type and the ΔGly-141 proteins (Fig. 6). The perturbation of the maxima of absorbance at ~ 380 and 450 nm and the intensity of the 380-nm peak appear to qualitatively reflect the increased interactions between the oxidized flavin and the residues in the 140s loop in the oxidized ΔGly-141 mutants. In the oxidized ΔGly-143 variant, the moderately altered spectrum is consistent with the highly disordered 140s loop, at least transiently interacting with the flavin and altering its microenvironment (Fig. 2).

Determination of the Redox Potentials of the FMN Domains

The redox potential of a protein is a major determinant of its function and activity. In flavodoxins, the potentials of the oxidized-semiquinone couple have been demonstrated to correlate with the H-bonding interaction of the flavin N5 proton (34). Because our mutants structurally perturbed the flavin N5 protein interaction, the midpoint potentials for the ox/sq and sq/hq couples for the separate FMN domain of WT CYPOR and the deletion mutants were investigated under anaerobic conditions. The potentials are summarized in Table 5 along with the potentials for WT CYPOR rabbit (57) and human CYPOR (29). Das and Sligar (58) determined the midpoint potentials for the ox/sq and sq/hq of the FMN of the soluble rat WT CYPOR at pH 7.4 to be −68 and −246 mV, respectively. These values are in agreement with the redox potentials obtained from this work for the FMN of the soluble diflavin WT rat CYPOR (−56 mV for FMNox/sq and −249 mV for FMN sq/hq) at pH 7.4. Previous experiments on diflavin reductases have shown that the potentials of the FMN domain are similar in the diflavin and separate flavin domains (29, 58, 59). Because of the confounding presence of both FAD and FMN in the diflavin CYPOR, the FMN redox potentials could not be unambiguously assigned for the diflavin ΔGly-143 and two ΔGly-141 mutants. The FMN domains were therefore engineered, expressed, and purified, and their potentials were measured under anaerobic conditions without interference from the FAD domain. Overall reduction was followed at 454–466 nm. The blue semiquinone and red semiquinone were evaluated at ~585 and ~390 nm, respectively. Fig. 7 shows the spectral changes observed during the titration of the FMN domains with dithionite. As expected, the potentials of the separate wild type FMN domain were similar to those obtained in the diflavin CYPOR (ox/sq −56 mV; sq/hq −249 mV) (Table 5). The FAD potentials for the diflavin wild type reductase were −280 mV for the ox/sq and −383 mV for the sq/hq couples in agreement with previous measurements (25, 29).

The FMN oxidized/semiquinone and the semiquinone/hydroquinone couples for the ΔGly-143 mutant (−235 and −297 mV, respectively, Table 5) are both more negative than those of the wild type and are consistent with an extremely

TABLE 5
Comparison of the redox potentials of the FMN domains of CYPOR and nNOS reductase domain

Reductase mutant/WT	$E_{ox/sq}$	$E_{sq/hq}$	pH	Ref.
	mV	*mV*		
Truncated rat WT CYPOR	−56 ± 7	−249 ± 14	7.4	This work
Truncated rat WT CYPOR	−68	−246	7.4	58
WT FMN domain	−56 ± 7	−252 ± 23	7.4	This work
Rabbit WT CYPOR	−110	−270	7	57
Truncated human CYPOR	−66 ± 8	−269 ± 10	7	29
ΔGly-141 FMN domain 388 nm	−229 ± 3	−53 ± 4	7.4	This work
E142N FMN domain	−37 ± 3	−237 ± 21		This work
ΔG141/E142N FMN domain 388 nm	−281 ± 21	−204 ± 2	7.4	This work
ΔGly-143 FMN domain	−235 ± 7	−297 ± 5	7.4	This work
P450 BM3 WT FMN domain	−240	−160	7	68
P450 BM3-G537 insert	−198	−245	7	43
Rat nNOS WT FMN domain	−179	−314	7.5	25
Rat nNOS ΔG810 FMN domain	−280	−190	7.5	25
Free FMN	−313	−101	7	9

weak and transient or no H-bond between the flavin N5 and the protein (Figs. 2 and supplemental Fig. S2). The lower potentials also suggest that the semiquinone as well as the hydroquinone are thermodynamically competent to reduce substrate-bound ferric cyt P450 (approximately −245 mV) (60). Note that the ΔGly-143 mutation maintains the oxidized/semiquinone couple at a more positive potential than the sq/hq couple and presumably more stable form.

In contrast, the sq and hydroquinone potentials in the ΔG141/E142N double mutant were reversed compared with the wild type protein (Table 5). For example, when followed at 388 nm, the oxidized/semiquinone couple (−281 mV) is lower and more negative than the semiquinone/hydroquinone couple (−204 mV), indicating that the FMN hydroquinone has a higher potential than the semiquinone and will therefore be more stable than the semiquinone. As a result, the FMN hydroquinone is likely to be thermodynamically incapable of reducing substrate-bound, ferric cyt P450 (approximately −245 mV) (60). Unexpectedly, the ΔGly-141 potentials were −229 mV for the ox/sq and −53 mV for the sq/hq couples, significantly different from the ΔG141/E142N double mutant. The potential determination for ΔGly-141 was repeated several times, and the data were analyzed excluding the data points that did not fall on the curve in Fig. 7. Irrespective of how the data were analyzed, the ΔGly-141 sq/hq couple was calculated to be −53 mV. Because we were concerned that the positive potential was not consistent with ΔGly-141's otherwise similarity both structurally and biochemically to the ΔG141/E142N mutant, the E142N FMN domain mutant was constructed, purified, and analyzed to determine whether the E142N mutation might be causing the potential difference between the two mutants. The potential of the E142N FMN domain (−37 and −237 mV for the ox/sq and sq/hq, respectively) is similar to wild type (Table 5) and does not obviously account for the difference in potentials between the ΔGly-141 and the ΔG141/E142N mutant. However, the Asn may be playing a different role in the WT and mutant. Data for the wild type FMN domain are not shown because they are similar to that for the E142N FMN domain. Lack of a stable red semiquinone in the ΔGly-141 mutants hampers the measurement and fitting process of the potential determination and may introduce uncertainties in the final values. Nevertheless, the conclusion that the hydroquinone of the ΔGly-141 mutants is the more positive high potential couple is confirmed by their functional and biochemical properties.

To summarize, the midpoint (sq/hq) potentials of both ΔGly-141 mutants are more positive than those of the ox/sq couples in the two ΔGly-141 FMN domains. A higher potential of the hydroquinone than the semiquinone is similar to what is observed in FMN in solution, the wild type P450 BM3 reductase, and the ΔGly-810 mutant of nNOS reductase domain (9, 43, 61, 62). The markedly different redox potentials of the two ΔGly-141 mutant proteins from the corresponding values of the wild type can be explained by the altered interaction between the flavin and the shortened 140s loop. In the oxidized form of the two ΔGly-141 mutants, two hydrogen bonds exist between the N5 and O4 of the flavin and the backbone amides of Glu-142 and Gly-143, respectively (in wild type numbering). These residues are now in the 141 and 142 positions in the deletion mutant (Figs. 3 and 4). The tighter loop and the formation of a hydrogen bond between the main chain amide nitrogen of Glu-142 (hydrogen donor) of the 140s loop and the oxidized flavin N5 (hydrogen acceptor) decrease the pK_a of N5 and inhibit the protonation of N5 in the one-electron-reduced semiquinone state at pH 7.4 (34). Consequently, unlike the wild type protein, which forms the stable neutral blue semiquinone, the Gly-141 deletion mutants form an unstable red anionic semiquinone that rapidly converts at equilibrium to the two-electron-reduced, higher potential hydroquinone. Note the absence of either red or blue semiquinone formation during the titration of the FMN domain with dithionite when the redox potentials were determined (Figs. 7 and 8). Withdrawal of electron density from the flavin hydroquinone by the H-bonds between the flavin and the amides of the residues now in positions 141 and 142 presumably stabilizes the mutant hydroquinone at the more positive potential than the FMN hydroquinone of the wild type protein (approximately −249 mV). In contrast, the protonated N5 of the wild type hydroquinone serves as an H-bond donor to the carbonyl of Gly-141, which provides electron density to the flavin, thereby causing its potential to be more negative. In the oxidized WT protein, there are no H-bonds between either the flavin, N5, O4, or the 140s loop. The aforementioned results indicate that the 140s loop is a major determinant of the flavin redox potentials. The length of the loop, its flexibility, and sequence modulate both

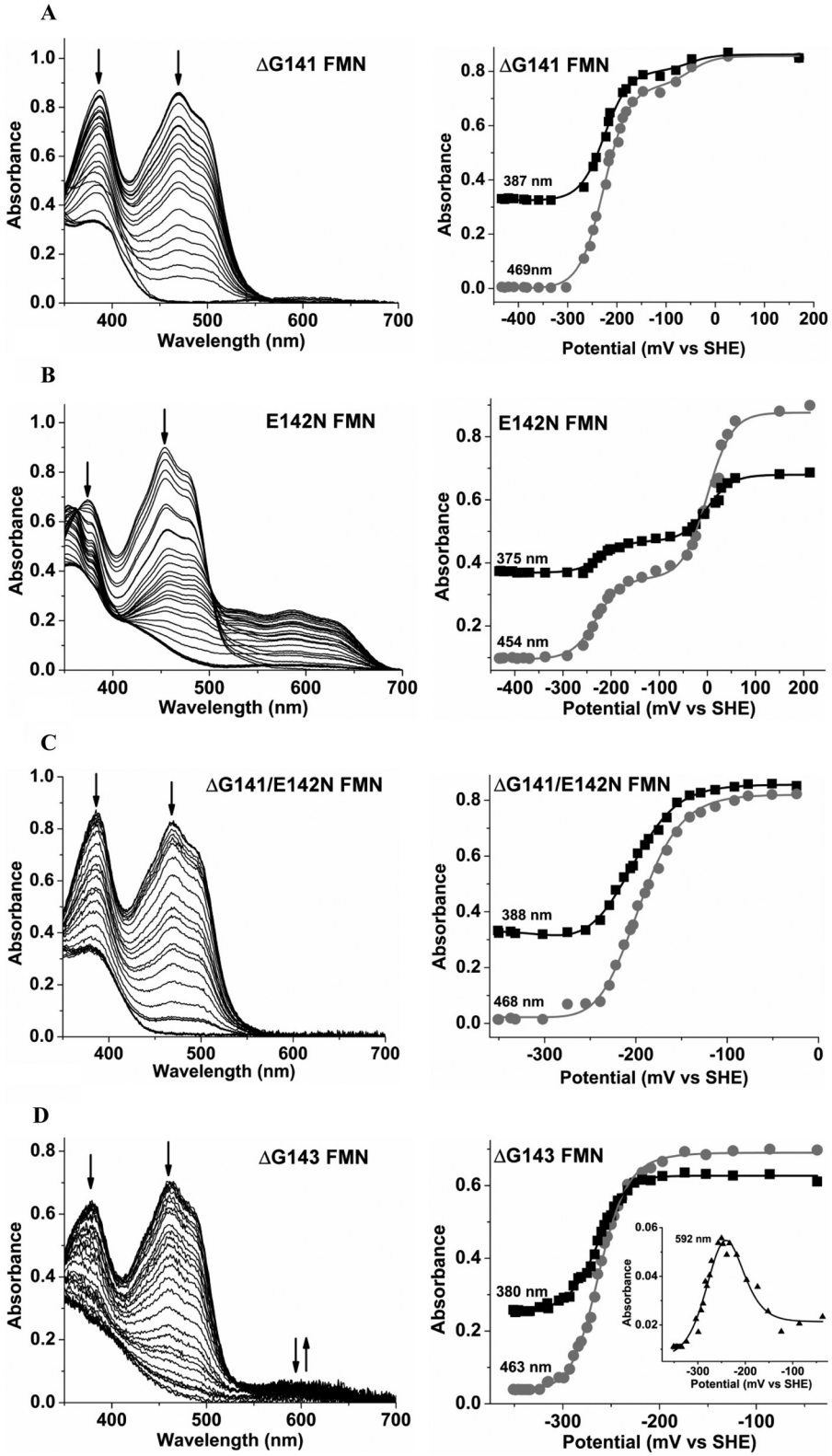

FIGURE 7. **Spectral changes and a plot of absorbance at the specified wavelengths *versus* the potential during titration of the separate mutant FMN domains with dithionite.** *A,* ΔGly-141. *B,* E142N. *C,* ΔG141/E142N. *D,* ΔGly-143. *Inset* shows absorbance changes at 592 nm during the titration.

the affinity of FMN for the apoprotein and thermodynamics and ultimately its catalytic activity. Shortening the loop at Gly-143 gives rise to a mutant with potentials intermediate between those of the ΔGly-141 mutants and the wild type. The potential for the ox/sq couple of the ΔGly-143 variant protein is approximately −235 mV (Table 5), significantly lower than that of the wild type protein (approximately −56 to −110 mV), consistent with the crystal structure that indicates a very mobile 140s loop

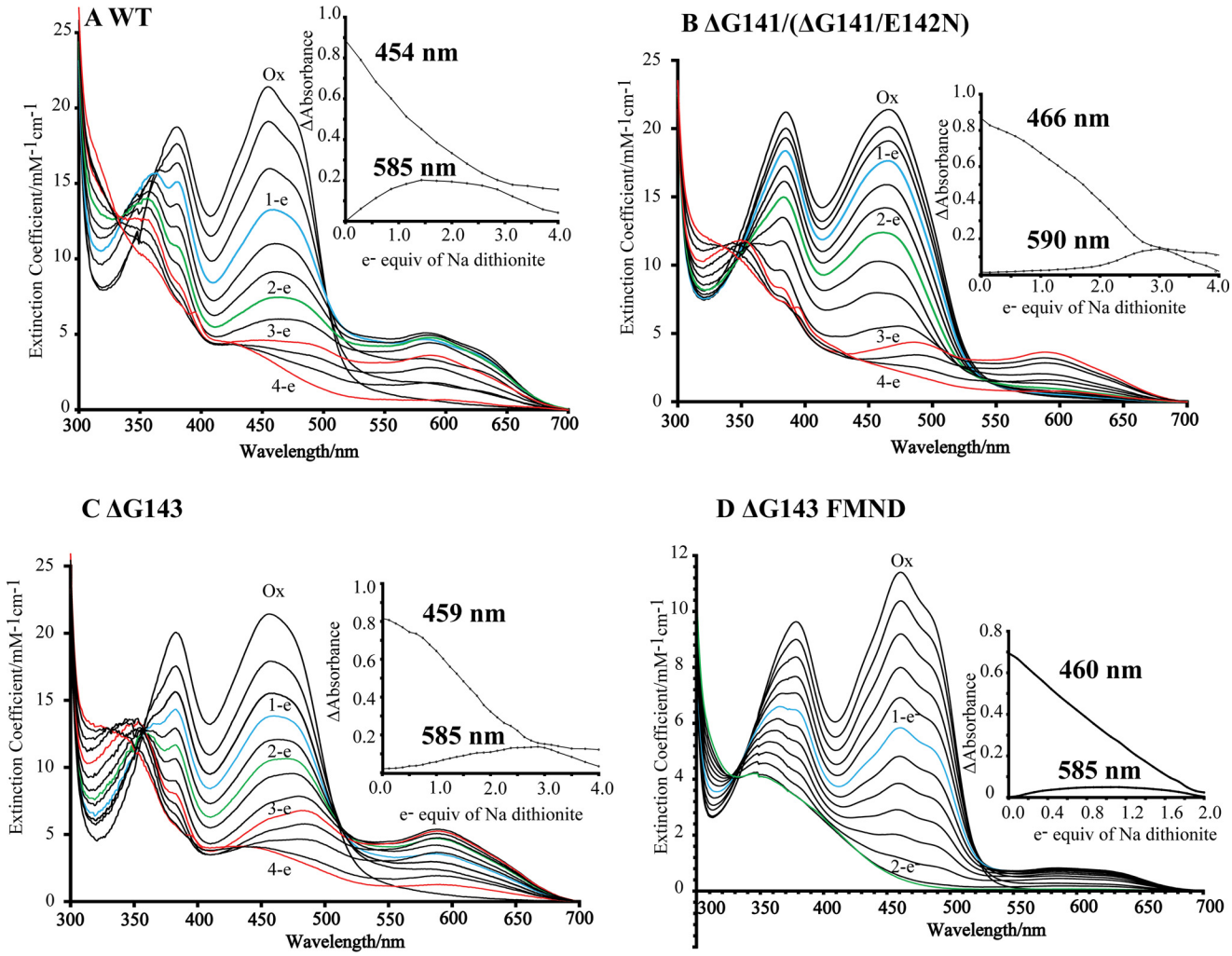

FIGURE 8. **Spectral changes of the diflavin wild type and glycine deletion mutants and the FMN domain of ΔGly-143 CYPOR during anaerobic titration with dithionite.** *Insets* plot the change in absorbance at 454–466 nm (overall reduction) and 585–590 nm (*blue semiquinone*) *versus* the electron equivalents of dithionite added. *A,* wild type. *B,* ΔG141. Because the spectral changes at equilibrium are the same for both the ΔGly-141 and ΔG141/E142N mutants, only a single data set is illustrated. *C,* ΔGly-143. *D,* FMN domain of ΔGly-143.

that does not stably interact with the flavin in either the oxidized or reduced form. Protonation of the N5 flavin in the semiquinone gives rise to a blue semiquinone as in the wild type. However, the blue semiquinone is presumably only partially and transiently stabilized by an H-bond between a mobile 140s loop carbonyl group and a reduced and protonated N5H. Similarity between the FMN hydroquinone potentials of the ΔGly-143 and wild type is also consistent with the presence of only transient electron-withdrawing H-bonds between the flavin and the 140s loop residues. Note that the FMN redox potential couples in the ΔGly-143 mutant (−235 mV, ox/sq and −297 mV, sq/hq) should thermodynamically allow the reduction of substrate-bound ferric cyt P450 (approximately −245 mV), see below.

Anaerobic Reduction of the Diflavin WT CYPOR and the Glycine Deletion Mutants with Sodium Dithionite

Wild Type—To confirm and extend our understanding of the molecular basis of the redox potential and assist in interpreting the kinetics of reduction by NADPH, the spectral changes occurring at equilibrium during anaerobic reduction of wild type and the diflavin mutant proteins by standardized sodium dithionite were investigated. The WT CYPOR undergoes four-electron reduction with sodium dithionite to generate the fully reduced enzyme in which both the FMN and FAD are in their anionic hydroquinone states. The one-electron reduced wild type enzyme is the air-stable FMN blue semiquinone (Fig. 8*A*), which exhibits a broad absorbance band at 585 nm and a shoulder at 630 nm. This FMN blue semiquinone shoulder at 630 nm is absent in FAD semiquinone and can be used as a spectral tool to distinguish between the two semiquinones (10). Both FMN and FAD form neutral blue semiquinones that have markedly different oxidized/semiquinone potentials (FMNox/sq, −56 mV and FAD ox/sq, −280 mV). The structure of the wild type reveals that the FMN N5H forms a strong hydrogen bond to the carbonyl of Gly-141, although the FAD N5H would be within a hydrogen bonding distance of the side chain hydroxyl of Ser-457 with which it likely forms a weaker hydrogen bond. This is consistent with the idea that the strength of the N5H interaction of the flavin with the protein modulates the potential of the flavin ox/sq couple. Upon addition of the first electron to wild type CYPOR, isosbestic points are formed at ~363 and ~503

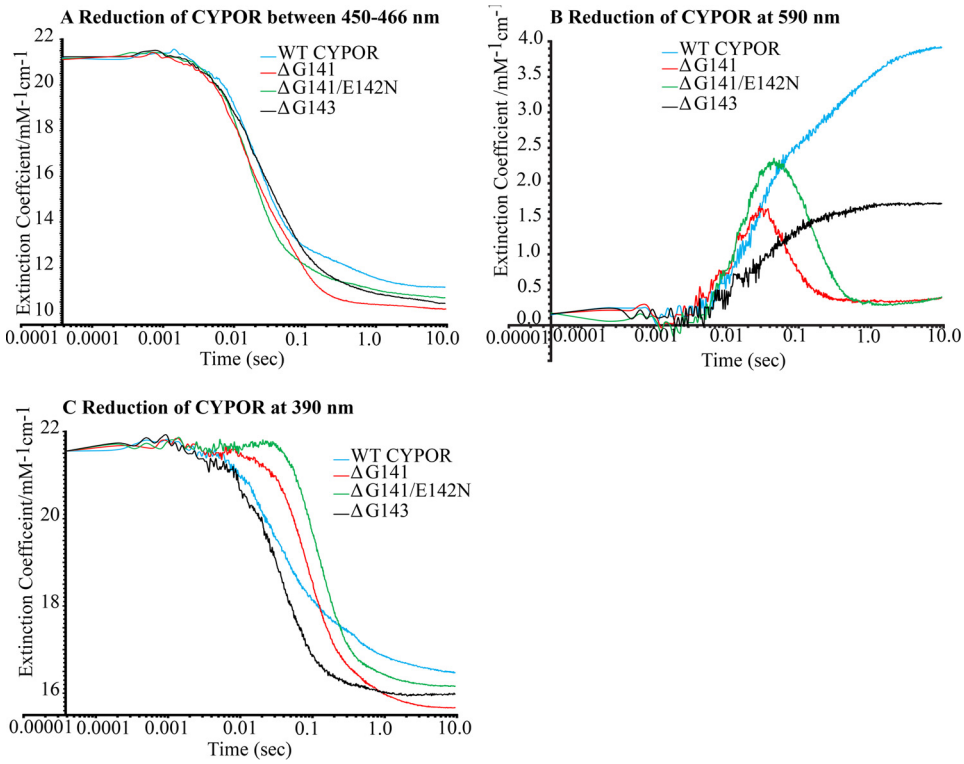

FIGURE 9. **Kinetic traces of the reduction of the diflavin wild type and three glycine deletion mutants of CYPOR by 1 molar eq of NADPH under anaerobic conditions at 25 °C.** *A,* kinetic traces at 450–466 nm (overall reduction). *B,* kinetic traces at 590 nm (*blue semiquinone*). *C,* kinetic traces at 390 nm (*red semiquinone*). See "Experimental Procedures" for details.

nm. Addition of a second and third electron to CYPOR causes a further decrease in the 454-nm band, which is accompanied by only a small decrease in the broad 585-nm band (see Fig. 8*A* indicating the coexistence of both the FMN hydroquinone and FAD semiquinone and the similarity of their potentials) (20, 29). The blue semiquinone begins to disappear with the addition of the fourth electron, which forms the FAD hydroquinone. An isosbestic point is observed at ~330 nm during this phase of titration until a fully reduced enzyme is obtained (four electrons added).

Δ*Gly-143*—The spectral changes during reduction of the ΔGly-143 mutant with sodium dithionite were different from those observed during the reduction of the wild type (Fig. 8, *A* and *C*). Simultaneous absorbance decreases reflecting overall reduction were observed at 459 and 382 nm (Fig. 8*C*). However, the addition of one-electron equivalent resulted in only a small amount of the neutral blue semiquinone that continued to accumulate, only peaking when three-electron equivalents had been added and decreasing as the fourth equivalent was added. This behavior suggests that the potential of the FMN blue semiquinone, FMN hydroquinone, and FAD blue semiquinone might not be widely separated and that these three species might coexist in solution (Fig. 8*C*). Surprisingly, there are also isosbestic points at ~358 and 510–515 nm between oxidized and one-electron-reduced, the one-electron and two-electron-reduced enzyme, and the two- and three-electron-reduced protein. These results are consistent with three species with distinguishable but similar redox potentials (Table 5).

Because it was not possible to unequivocally determine whether the observed blue semiquinone was that of FMN or FAD, the separate FMN domain (residues 57- 240) of the ΔGly-143 protein was constructed, purified, and investigated. As can be seen in Figs. 8*C* and 7*D*, reduction of the ΔGly-143 FMN domain with one-electron equivalent revealed formation of a small amount of blue semiquinone with approximate isosbestic points at 345 and 515 nm, which indicates that the potentials of the blue semiquinone and hydroquinone would not be very different, resulting in the coexistence of the FMN semiquinone and hydroquinone in solution. This indicates that residues in the disordered 140s loop observed in the structure of the ΔGly-143 mutant most likely transiently stabilize a protonated N5H FMN blue semiquinone. There was no evidence for formation of a stable red semiquinone.

Δ*Gly-141 and* Δ*G141/E142N*—Reduction of the FMN domains of the diflavin ΔGly-141 and ΔG141/E142N deletion mutants under anaerobic conditions with sodium dithionite occurred with similar spectral changes that were significantly different from the wild type and ΔGly-143 mutant. In contrast, the spectral changes during reduction of the FAD domains in the diflavin proteins of the three mutants and WT were all similar indicating that the mutations in the FMN domain did not affect the FAD domain (Fig. 8, *A*–*C*). Addition of the first two electrons occurred with absorbance decreases at 385 and 466 nm but without accumulation of a blue semiquinone at 585 nm (Fig. 8*B*). There are, however, isosbestic points at ~340–345 and 546 nm between the oxidized and two-electron-reduced reductase. This is consistent with the formation of an FMN hydroquinone with a higher potential than that of the unstable FMN semiquinone (Table 5). Addition of the third electron generated a small increase in absorbancy at 580 nm

TABLE 6
Kinetics of reduction of wild-type and glycine deletion mutants of CYPOR by 1 eq of NADPH at 25 °C
A is amplitude.

Reductase	λ/nm	A1 (%)	k_1	A2 (%)	k_2
			s^{-1}		s^{-1}
WT CYPOR	390	78.0 ± 0.4	46.7 ± 2.8	22.0 ± 0.4	3.4 ± 0.2
	452	84.5 ± 0.6	42.1 ± 0.4	15.6 ± 0.6	2.4 ± 0.1
	590	79.9 ± 0.4	38.3 ± 2.2	20.2 ± 0.4	1.3 ± 0.5
ΔGly-141	390	100	12.9 ± 0.3		
	466	55.0 ± 2.1	55.2 ± 4.8	44.9 ± 2.1	8.6 ± 0.4
	590		50.8 ± 3.7		21.9 ± 1.6 (Decay)
ΔG141/E142N	390		47.5 ± 3.5		7.9 ± 0.2 (Decay)
	466	85.5 ± 0.9	57.1 ± 1.2	14.5 ± 0.9	4.7 ± 0.3
	590		53.6 ± 1.6		7.3 ± 0.1 (Decay)
ΔGly-143	390	75.0 ± 1.6	43.5 ± 0.7	25 ± 1.6	6.0 ± 0.1
	459	68.4 ± 2.2	43.5 ± 1.7	31.6 ± 2.2	6.9 ± 0.7
	590	74.6 ± 1.2	33.4 ± 0.8	25.4 ± 1.2	2.6 ± 0.8

due to the putative FAD blue semiquinone with an isosbestic point at ~358 nm, which occurred between the addition of the third and fourth electron. The similarity of the spectral changes for the two ΔGly-141 mutants upon addition of an equivalent amount of sodium dithionite indicates that the charge of the residue replacing Gly-141 in the shortened loop (Glu-142 *versus* Asn-142) does not alter the conclusion that the hydroquinone is more stable in both proteins. Reduction by sodium dithionite is thought to be via the one-electron reductant, $SO_2^{\cdot-}$, a radical species (63); therefore, in both ΔGly-141 mutants, an FMN semiquinone species was likely formed transiently. The absence of a measurable amount of blue FMN semiquinone with the addition of 2 molar electron eq suggests that an unstable red semiquinone was formed and that it rapidly accepts a proton and a second electron to form the FMN hydroquinone and oxidized FAD (63). These results are consistent with the structure of the ΔGly-141 mutants and the biochemical results with the separate ΔGly-141 FMN domains.

Kinetics of the Pre-steady-State Reduction of WT and Mutant CYPOR by 1 Molar Eq of NADPH

In an effort to determine whether formation of the high potential FMN hydroquinone of the ΔGly-141 mutants proceeded via formation of an unstable anionic red semiquinone as their redox potentials suggested, the pre-steady-state kinetics of reduction of the wild type and deletion mutants by 1 molar eq of NADPH under anaerobic conditions was investigated. The reduction was followed at three wavelengths as follows: absorbance at 450–466 nm reports primarily on overall reduction; at 590 nm the blue semiquinone formation was evaluated; and the 390 nm absorbance provides information about the red semiquinone (Fig. 9).

Reduction of Wild Type CYPOR

The kinetic traces and the rate constants for the kinetics of reduction of WT CYPOR by 1 molar eq NADPH are shown in Fig. 9 and Table 6. When followed at 452 nm, the reduction of the WT CYPOR results in biphasic bleaching of the flavin absorbance (Fig. 9). The first rapid phase (k_1 = 42.1 s^{-1}) represents the reduction of FAD by NADPH and transfer of an electron from the FAD hydroquinone to FMN as shown by the simultaneous formation of a FAD and FMN blue semiquinone at 590 nm (k_1 = 38.3 s^{-1}). The process responsible for the slower second phase (k_2 = 2.4 s^{-1}) at 452 nm is not well understood. The reduction of wild type CYPOR at 390 nm (Fig. 9*C*) was also fitted to a biphasic function, and the fast phase (k_1 = 46.7 s^{-1}) is similar to that observed at 452 nm and reflects reduction of FMN and FAD. Following reduction of wild type CYPOR by 1 molar eq of NADPH, the mixture of reductase molecules is expected to consist of an equilibrium mixture of both the disemiquinone FAD_{sq}/FMN_{sq} and FAD_{ox}/FMN_{hq}, where the major species is the FAD_{ox}/FMN_{hq} (20).

Reduction of the ΔGly-143 Mutant

The kinetics of reduction of the ΔGly-143 mutant by 1 molar eq of NADPH were also monitored at 390, 459, and 590 nm (Table 6 and Fig. 9). The biphasic rate constant at 459 nm for the first phase for ΔGly-143 mutant (k_1 = 43.5 s^{-1}) is similar to that of the wild type CYPOR (k_1 = 42.1 s^{-1}) and represents a hydride transfer to FAD and subsequent electron transfer to the oxidized FMN. The rate of interflavin electron transfer and blue semiquinone formation, which was monitored at 590 nm, is slightly slower than that of WT CYPOR (k_1 = 33.4 s^{-1} *versus* k_1 = 42.1 s^{-1}) with ~60% less accumulation of the stable blue semiquinone. A result of the only ~60 mV difference between the ΔGly-143 semiquinone and the hydroquinone potentials is that both the semi-and hydroquinone will coexist in solution. The slightly slower rate of interflavin electron transfer probably reflects the decreased thermodynamic driving force and possibly steric hindrance by the extremely mobile 140s loop. As expected, the rate of reduction of the flavin of ΔGly-143 at 390 nm (Fig. 9*C*) was biphasic and similar to that observed at 459 nm (k_1 = 43.5 s^{-1}). The absence of an extended duration of absorbance at 390 nm is consistent with the lack of formation of red semiquinone.

Reduction of the ΔGly-141 Mutants

The kinetics of reduction of the ΔGly-141 mutants by 1 molar eq of NADPH were followed at 390, 466, and 590 nm, and the rate constants are summarized in Table 6. When followed at 466 nm (Fig. 9*A*), the rate constant for the fast phase (k_1 ~56 s^{-1}) for both ΔGly-141 mutants represents reduction of FAD by NADPH. This rate constant for ΔGly-141 mutants is slightly higher than that observed for wild type CYPOR. Because there is no detectable difference in the relative orientation of and distance between FAD and FMN among wild type and ΔGly-141 mutants structures, the ~20% (56 *versus* 42 s^{-1}) faster rates for ΔGly-141 mutants were not due to better geometrical

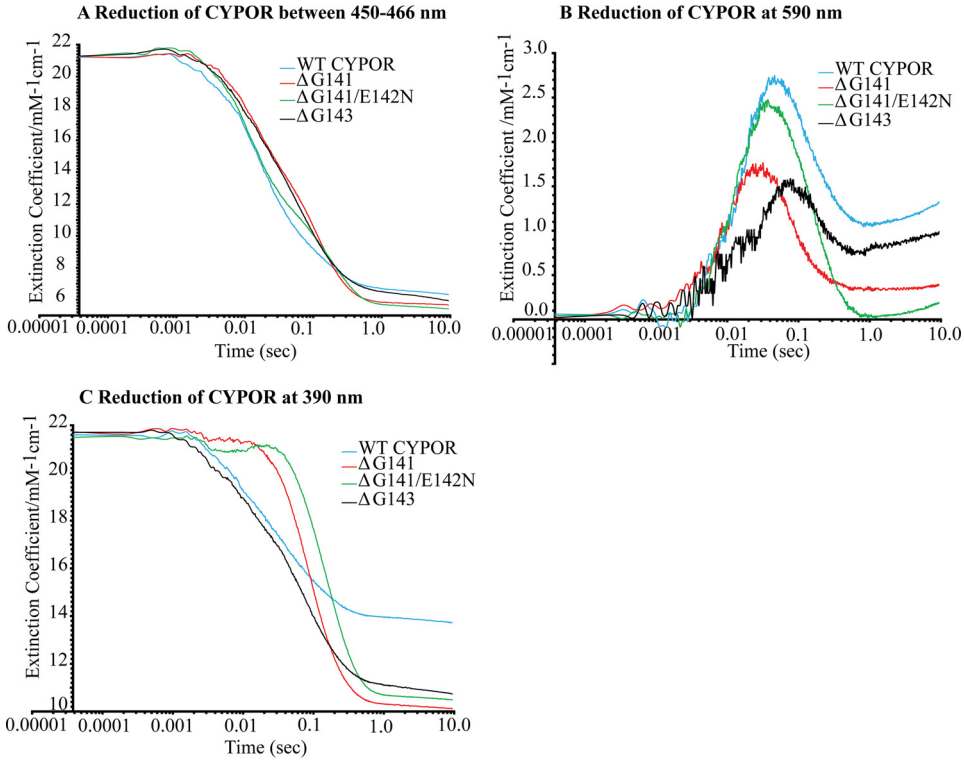

FIGURE 10. **Kinetic traces of the reduction of the diflavin wild type and three glycine deletion mutants of CYPOR by 10 molar eq of NADPH under anaerobic conditions at 25 °C.** *A,* kinetic traces at 450–466 nm (overall reduction). *B,* kinetic traces at 590 nm (*blue semiquinone*). *C,* kinetic traces at 390 nm (*red semiquinone*). See "Experimental Procedures" for details.

arrangements of the two flavins. These faster rates probably reflect a greater thermodynamic driving force for rapidly forming the high potential FMN hydroquinone. The FAD blue semiquinone at 590 nm for ΔGly-141 and ΔG141/E142N peaks at ~30–40 ms with rate constants of ~52 s^{-1} and then monophasically decays to the FMN hydroquinone and oxidized FAD with rate constants of 21.9 and 7.3 s^{-1}, respectively (Table 6 and Fig. 9*B*). It is proposed that immediately after mixing the ΔGly-141 reductases with NADPH, a hydride ion is transferred to FAD which quickly disintegrates one-electron at a time into the stable FMN hydroquinone and oxidized FAD, via a blue FADsq-red anionic FMNsq intermediate. Because our ΔGly-141 mutants did not form a stable blue FMN semiquinone, we turned our attention to stopped-flow spectrophotometric studies at 390 nm in an attempt to indirectly capture the red semiquinone formation and its decay in the mutants (Fig. 9*C*; Table 6). In stark contrast to the wild type and ΔGly-143 mutant, the absorbance at 390 nm did not bleach at the same rate as the absorbance at 454–466 nm. The slow absorbance decay at 390 nm with both ΔGly-141 mutants has been attributed to the formation of the anionic red semiquinone species that has a maximum at 390 nm ($\epsilon \cong 16.5\ mM^{-1}\ cm^{-1}$) (1, 10, 23, 43). The rate of absorbance decrease in the ΔGly-141 and ΔG141/E142N mutants at 390 nm ($k = 12.9 \pm 0.3$ and $7.9 \pm 0.2\ s^{-1}$, respectively) is the net result of red semiquinone formation (at 390 nm), and the decrease in absorbance is due to flavin reduction (at 385 nm). It is noteworthy that the red FMN semiquinone persists for a longer time in the ΔG141/E142N mutant than the ΔGly-141 mutant that possesses an acidic glutamic acid at residue 141 One possible explanation for the increased stability of the red semiquinone is that the more rigid 140s loop in the double mutant sterically hinders protonation of the FMN N5, which is essential for further reduction to the hydroquinone. A second possibility is that the negative charge on the glutamic acid further destabilizes the red semiquinone and facilitates more rapid hydroquinone formation. A third more likely scenario is that the occurrence of a Glu instead of the highly preferred Asn in the $i + 1$ corner position of the type I′ β-turn destabilizes the loop and weakens its interaction with the FMN (49), consistent with the higher average *B*-factor of the loop and two conformations of the side chains of Tyr-140 and Glu-142 in the ΔGly-141 mutant (Fig. 3 and supplemental Fig. S3). As mentioned previously, the basis of the stability of Asn in the $i + 1$ position of the turn appears to be the ability of the side chain carbonyl of Asn to form a dipolar bond with the carbonyl carbon of Tyr-140 (53).

Kinetics of CYPOR Reduction by 10 Molar Eq of NADPH

To gain additional insight into the mechanism of electron transfer by the glycine deletion mutants, we investigated the kinetics of reduction of the WT reductase and the deletion mutants by a 10-fold excess of NADPH (Table 7 and Fig. 10). The reduction of CYPOR with a 10-fold excess of NADPH can be summarized as shown in Scheme 1. Because of additional reduced species and more complete reduction of the reductases, the kinetics of reduction with the 10-fold molar NADPH excess were also more complex (Fig. 10). Nevertheless, they confirm and extend the conclusions drawn from experiments with the 1 molar eq of NADPH. Overall, the initial rates of reduction with a 10-fold excess of NADPH were on average

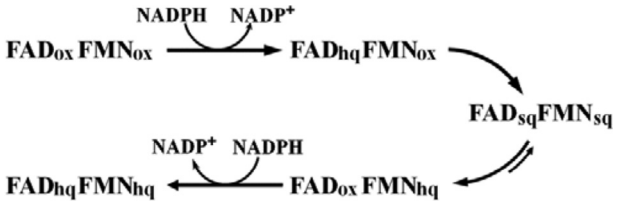

SCHEME 1.

~40% faster than reduction by an equimolar amount of NADPH (Tables 6 and 7). The absolute amount of blue semiquinone observed was also less (compare Figs. 9 and 10). In the ΔGly-143 mutant, the rate of formation of the blue FAD semiquinone, which measures interflavin electron transfer, remained ~30% slower (42 s^{-1}) than the reduction of the FAD domain itself (60 s^{-1}) irrespective of NADPH concentration. As proposed above, a decreased driving force (ΔGly-143 semiquinone −235 mV *versus* −56 mV for the WT) and perhaps steric hindrance due to a more mobile 140s loop contribute to this decreased rate of electron transfer between FAD and FMN.

In contrast, interflavin electron transfer from FAD to FMN was faster in the ΔGly-141 mutants compared with wild type and ΔGly-143 likely because of an increased thermodynamic driving force for a two-electron reduction to the FMN hydroquinone. Reduction by a second molecule of NADPH yields both FAD and FMN hydroquinones. Reduction of both ΔGly-141 mutants proceeds via formation of an evanescent anionic red FMN semiquinone as shown by an ~20–40-ms lag in the decrease in absorbance at 390 nm (Fig. 10*C*) compared with the more rapid bleaching beginning at ~2 ms in the wild type and ΔGly-143 mutant. Slightly less blue semiquinone was observed during the reduction of the ΔGly-141 mutants by a 10-fold molar excess *versus* 1 eq of NADPH likely because of a more rapid and extensive formation of the FMN hydroquinone, depletion of the FAD semiquinone, and reformation of the oxidized FAD, which can be reduced by a second molecule of NADPH (Scheme 1) (compare Figs. 9 and 10). Interflavin electron transfer from FAD to FMN was slightly faster (~67–74 s^{-1}) in the ΔGly-141 variants than the WT and ΔGly-143 (~42 s^{-1}). Whether the potentials and/or the structure and dynamics of the 140s loop influence this rate remains to be determined.

Activity of the Mutant Reductases with Redox Partners, Cyt P450 2B4, Cytochrome c, and Ferricyanide

In view of the mutant's altered redox potentials and kinetic behavior during steady-state and presteady-state reduction with dithionite and NADPH, respectively, the ability of the mutant proteins to catalyze the metabolism of the model substrate, benzphetamine, by cyt P450 2B4 was tested (Table 8). The ΔGly-143 deletion retained ~20% of wild type activity. This indicates that the interaction between FMN and the 140's loop of CYPOR is a major determinant of the ability of CYPOR to support cyt P450 catalysis. Thermodynamically, both the FMN semiquinone (−235 mV) and hydroquinone (−297 mV) of ΔGly-143 should allow transfer of electrons to the ferric heme of benzphetamine-bound cyt P450 (−245 mV), albeit that the driving force for the hydroquinone would be greater.

In contrast, the ΔGly-141 deletion mutants are essentially inactive, less than 5% of the wild type activity, with cyt P450 2B4. The FMN hydroquinone redox potential of the ΔGly141 deletion mutants is more positive and is not likely to be thermodynamically capable of normally transferring electrons to the heme of substrate-bound ferric cyt P450 2B4 (−245 mV). Although the red semiquinone is thermodynamically poised to reduce ferric cyt P450, it is unstable under the experimental conditions. These results indicate that an appropriate redox potential is necessary but not sufficient for normal reductase activity (Table 8).

The high potential mitochondrial protein, cyt *c* (approximately +250 mV), has long been used as an artificial substrate for reductase assays because of the simplicity and rapidity of the assay (64). The mutants were assayed for their ability to reduce cyt *c*. The FMN hydroquinone of the wild type CYPOR, not the blue FMN semiquinone, reduces cytochrome *c* (cyt *c*), although it is the red anionic FMN semiquinone of cyt P450 BM3 that reduces cyt *c* (Table 8). Although the ΔGly-143 mutant is ~33% less active with cyt *c*, both ΔGly-141 mutants exhibit wild type activity with cyt *c*. Because both the ΔGly-143 blue semiquinone (−235 mV) and hydroquinone (−297 mV) are thermodynamically capable of reducing cyt *c*, it was surprising that they were less active than the wild type protein. A likely and at least partial explanation for the unexpected differences in activities of the ΔGly-141 mutants with cyt *c* and cyt P450 2B4 is that the low potential short lived red semiquinone of the ΔGly-141 mutants can rapidly transfer electrons to the high potential cyt *c*. However, the red semiquinone may decay before it is able to reduce ferric cyt P450 2B4 in a much slower reaction (k ~6.7 s^{-1}), whereas the ΔGly-141 mutant hydroquinones are both unstable and thermodynamically inappropriate (37).

As a control, the mutant reductases were also assayed for their ability to reduce ferricyanide, which is considered to be reduced exclusively by the FAD domain (Table 8) (21). In the presence of NADPH, all three mutants are able to reduce ferricyanide to the same extent as wild type CYPOR. This indicates that reduction of FAD by NADPH, *i.e.* the hydride transfer step from NADPH to FAD, occurs normally in all three mutants and that the mutations in the FMN domain did not perturb this step of catalysis.

Comparison of the Autoxidation of the Two-electron-reduced Wild Type and Mutants in the Diflavin Protein and the FMN Domain

In an effort to gain deeper insight into the biochemical basis of the altered activity of the mutants with cyt P450 2B4 and cyt *c* under aerobic conditions, the rate of autoxidation of the mutants, which had been two-electron-reduced, was investigated in both the diflavin enzyme and the FMN binding domain. Experiments were conducted with the FMN domain because of uncertainties in interpretation of the results with the intact protein, especially with ΔGly-143. Tables 9 and 10 and Fig. 11, *A* and *B,* reveal that oxygen readily transforms all three two-electron-reduced mutants directly to the oxidized protein, indicating that both the red and blue mutant semiquinones were unstable. In contrast, the WT oxidized to a stable blue semiquinone. With the exception of ΔGly-141, the rate of autoxidation was slower in the diflavin construct of the other

TABLE 7
Kinetics of reduction of wild-type CYPOR and glycine deletion mutants by 10 molar eq of NADPH

Reductase	λ/nm	A1 (%)	k_1	A2 (%)	k_2
			s^{-1}		s^{-1}
WT CYPOR	390	50.2 ± 0.1	66.7 ± 1.3	49.8 ± 0.1	6.1 ± 0.1
	452	67.3 ± 1.0	60.7 ± 1.7	32.7 ± 1.0	6.4 ± 0.4
	590		54.9 ± 3.3		7.2 ± 0.8 (Decay)
ΔGly-141	390				7.8 ± 0.5 (Decay)
	466	36.5 ± 0.7	82.4 ± 4.6	63.5 ± 0.7	7.9 ± 0.2
	590		73.6 ± 3.2		14.7 ± 0.4 (Decay)
ΔG141/E142N	390	19.1	40.1 ± 2.3	68.98	7.5 ± 0.2 (Decay)
	466	56.5 ± 0.4	80.6 ± 2.5	43.5 ± 0.4	5.4 ± 0.1
	590		66.8 ± 1.8		6.8 ± 0.2 (Decay)
ΔGly-143	390	40.2	60.6 ± 2.5	59.8	7.3 ± 0.4 (Decay)
	459	43.5 ± 1.4	61.5 ± 2.7	56.5 ± 1.4	8.4 ± 0.2
	590		41.9 ± 2.0		5.8 ± 0.2 (Decay)

TABLE 8
Activity of wild-type and CYPOR deletion mutants with redox partners
The activity of reductases with their model redox partners, cytochrome *c*, cytochrome P450 2B4, and ferricyanide was determined at 30 °C as described under "Experimental Procedures."

CYPOR reductase mutant/WT	Cytochrome *c*, nmol cyt *c* reduced/s/nmol CYPOR	Cytochrome P450 2B4, nmol CH_2O/s/nmol CYPOR	$Fe^{3+}(CN)_6^{-3}$, nmol reduced/s/nmol CYPOR
WT CYPOR	93.7 ± 0.2	0.73 ± 0.043	136 ± 3.4
ΔGly-141	88.5 ± 0.5	0.03 ± 0.002	122 ± 6.9
ΔG141/E142N	87.3 ± 0.6	0.02 ± 0.004	129 ± 8.6
ΔGly-143	51.0 ± 2.5 (62.2 ± 3.0) when corrected for FMN content	0.14 ± 0.011	130.4 ± 3.4

TABLE 9
Summary of rate constants and amplitudes for autoxidation of two-electron-reduced diflavin WT CYPOR, ΔGly-141, ΔG141/E142N, and ΔGly-143 by oxygen

	λ/nm	A1 (%)	k_1	A2 (%)	k_2
			s^{-1}		s^{-1}
WT CPR	452	100	0.026 ± 0.004		
	590	100	0.031 ± 0.001		
ΔGly-141	466	100	0.15 ± 0.01		
	590	100	0.15 ± 0.02		
ΔG141/E142N	466	100	0.026 ± 0.002		
	590	100	0.025 ± 0.001		
ΔGly-143	459	74	2.65 ± 0.07	26	0.04 ± 0.01
	590		2.20 ± 0.01		0.05 ± 0.01

TABLE 10
Summary of rate constants and amplitudes for autoxidation of the two-electron-reduced FMN domain of WT CPR, ΔGly-141, ΔG141/E142N, and ΔGly-143 by oxygen

Reductase	λ/nm	A1 (%)	k_1	A2 (%)	k_2
			s^{-1}		s^{-1}
WT CPR	452	100	0.54 ± 0.01		
	585	100	0.60 ± 0.007		
ΔGly-141	390	100	0.15 ± 0.01		
	469	100	0.15 ± 0.02		
ΔG141/E142N	390	100	0.083 ± 0.003		
	469	100	0.087 ± 0.001		
ΔGly-143	460	77	11.55 ± 0.47	23	1.91 ± 0.007
	585		21.95 ± 1.29		1.66 ± 0.07

three proteins than in the corresponding FMN domains, suggesting that the "closed conformation," where the two flavins are in close contact, hinders the FMN reactivity with oxygen (26). Superoxide is the inferred product of the reaction because access to the flavin C4a atom is sterically hindered and flavodoxins have generally been observed to form superoxide, not hydrogen peroxide, which rapidly dismutates to hydrogen peroxide (65). The diflavin protein of the double ΔG141/E142N mutant is more resistant to oxidation ($k = 0.026\ s^{-1}$) than the ΔGly-141 variant ($k = 0.15\ s^{-1}$). However, both decay monophasically within seconds to the oxidized enzyme without formation of a detectable semiquinone (Fig. 11). It is proposed that oxidation of the hydroquinone of the ΔGly-141 mutants of the two-electron-reduced occurs in two one-electron steps with the hydroquinone losing the first electron. This is instantaneously followed by a concerted deprotonation and loss of the second electron from the evanescent anionic semiquinone, which is more susceptible to oxidation than the neutral blue semiquinone (66). The two-electron reduced diflavin ΔGly-143 mutant is likely a mixture of two different reductase species (FMN_{sq}-FAD_{sq} and FMN_{hq}-FAD_{ox}). The anionic ΔGly-143 FMN hydroquinone will presumably donate an electron to oxygen forming a blue semiquinone. The FAD and FMN semiquinones would then undergo a concerted deprotonation and electron transfer from the FMN and FAD semiquinones to oxygen. The wild type FMN domain simply oxidizes by loss of an electron to form the air stable blue semiquinone and superoxide. These autoxidation data are difficult to reconcile with a semiquinone/hydroquinone potential of the ΔGly-141 mutant of −53 mV (Table 5), because the midpoint potential of the O_2/O_2^- couple is approximately −161 mV (67). In comparison, the hydroquinone of the P450 BM3 FMN domain is more stable and autoxidized much slower with a half-life of ~1 h (63).

Effect of pH on the Kinetics of the Formation and Decay of the Red Semiquinone of the ΔG141/E142N FMN Domain

The stability of the red semiquinone of ΔG141/E142N was probed using stopped-flow spectrophotometry at pH 7 and 9 by determining its rate of formation in the presence of excess dithionite and subsequent protonation and hydroquinone formation (Fig. 12). These experiments were performed to support our inference, in a more quantitative manner, that a red semiquinone was transiently formed during steady-state reduction of the ΔGly-141 mutants. Notice that reduction of the FMN domain by a 10-fold molar excess of dithionite, in the absence of the mediator methyl viologen, is markedly slower

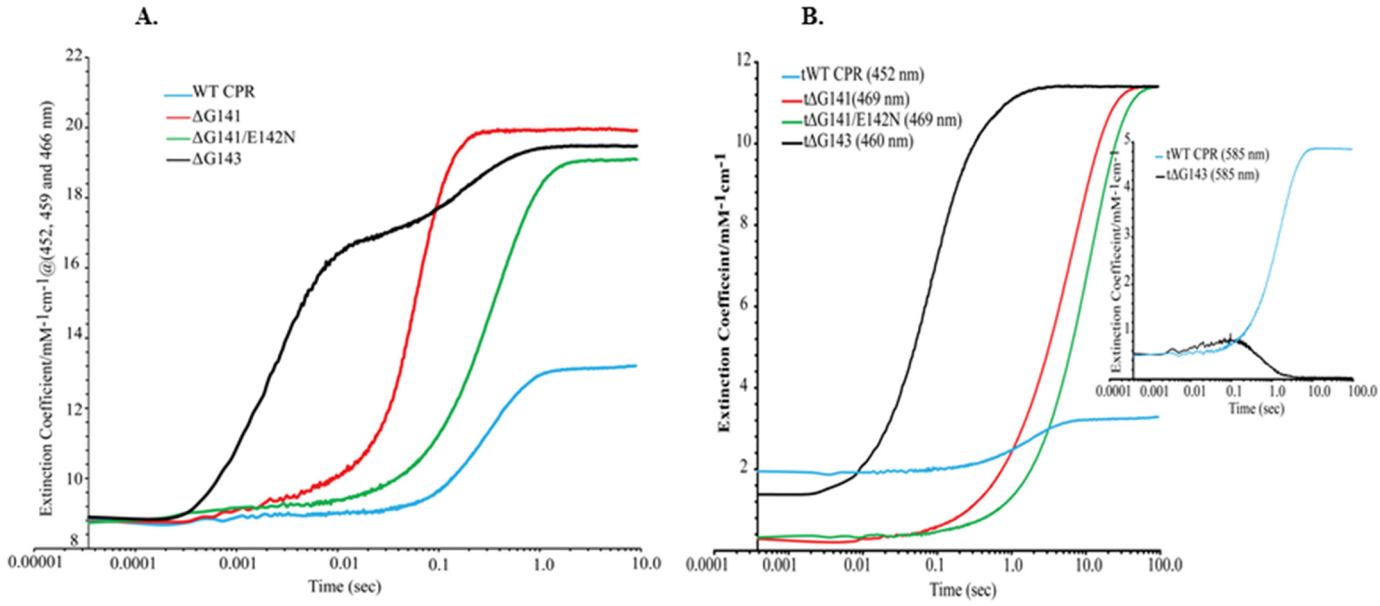

FIGURE 11. **Kinetics of the autoxidation of the two-electron-reduced diflavin and FMN domains of the wild type and three glycine deletion mutants at 25 °C.** The reaction was monitored at the absorbance maximum of each protein as follows: wild type (452 nm); ΔGly-143 (459 nm); ΔGly-141l and ΔG141/E142N (466 nm). *A*, diflavin proteins; *B*, FMN domains. The *inset* compares blue semiquinone formation and decay during autoxidation of the wild type and the ΔGly-143 mutant hydroquinone at 585 nm.

(Fig. 12, ΔG141/E142N $k \cong 0.44\ s^{-1}$) than the FMN reduction by a 1 molar eq of NADPH in the intact protein ($k \cong 57\ s^{-1}$) (Fig. 9 and Table 6), possibly because the reductant anionic sulfite (SO_2^-) is hindered from reacting with the flavin by the negative protein potential encircling the flavin at both pH 7 and 9. At pH 7, there was no evidence of red semiquinone formation with either the WT or mutant FMN domain. In contrast, at pH 9, the FMN domain of the mutant exhibited an increase in absorbance at 390 nm indicating formation of a red semiquinone ($k \cong 0.48\ s^{-1}$). This was quickly ($k \cong 0.12\ s^{-1}$) followed by bleaching at 390 nm, which represents the protonation of the semiquinone and further reduction of the mutant to the hydroquinone. As expected, the WT showed no sign of red semiquinone formation. It only exhibited a simultaneous decrease in absorbance at 390 and 454 nm at both pH 7 and 9 (Fig. 12). The ΔGly-141 mutant is presumed to have also proceeded to the hydroquinone via a red semiquinone which is less stable than the double mutant. These results are consistent with an estimated pK_a value of the mutant somewhat lower than pH 9 and a WT pK_a value greater than that of the mutants. The pK_a value of the blue semiquinone in a flavodoxin has been estimated to exceed 13.5 (34).

Comparison of the stability of the rat CYPOR double mutant red semiquinone with that of the corresponding reductase domain of P450 BM3 and the ΔGly-810 mutant of the nNOS reductase demonstrates that the rat CYPOR red semiquinone is much less stable than the anionic red semiquinone of the nNOS mutant and the P450 BM3 reductase. For example, the ΔGly-810 semiquinone of nNOS is stable for more than 50 s at pH 9 (25). At pH 8, the P450 BM3 reductase semiquinone is stable for greater than 10 min (68). These experiments reveal that the 140s loop is critical for flavin function but also illustrate that the local environment of the protein plays a role in ensuring that the flavin reactivity is matched to the catalytic properties required of the enzyme.

Discussion

To provide a more general understanding of the critical factors governing the reactivity of P450 reductase, the intrinsic activity of the flavin is described followed by a general description of how the protein environment tunes the intrinsic properties of the flavin. In a pH 7, an anaerobic aqueous solution of flavin to which one-electron equivalent has been added, less than 5% of the flavin exists as a blue semiquinone (pK_a 8.3). The blue semiquinone is generated by one-electron reduction of the flavin followed by protonation, essentially a proton-coupled electron transfer reaction. The remaining ~95% of the flavin exists as an equimolar mixture of the oxidized flavin and the more stable two-electron-reduced hydroquinone. Thus, neither the blue semiquinone nor the red semiquinone is intrinsically stable (1, 6). To carry out the transfer of a single electron, it is necessary for the flavoenzyme to create an environment that will stabilize a semiquinone and provide the flavin chemistry essential for a specific enzymatic reaction. One way to stabilize a protonated neutral blue semiquinone is to enhance H-bond formation between the donor, N5H, and a H-bond acceptor, a carbonyl or hydroxyl group on the protein. The strength of the H-bond can be varied to enhance the stability of blue semiquinone and thereby increase its pK_a value to the extent appropriate for enzymatic activity. Along with an increase in the pK_a value, the stabilization of the positive charge on the flavin will primarily increase the potential of the oxidized/semiquinone couple. The FMN and FAD of WT CYPOR, ΔGly-143 flavins, and flavodoxins employ this mechanism. In contrast, stabilization of the anionic unprotonated one-electron-reduced flavin dictates that protonation be prevented and that the negative charge on the flavin will be attenuated by an interaction with an NH_2 group from a backbone amide or even a basic amino acid side chain (Lys) on the protein. This interaction will result in a decrease in the pK_a value of the flavin N5.

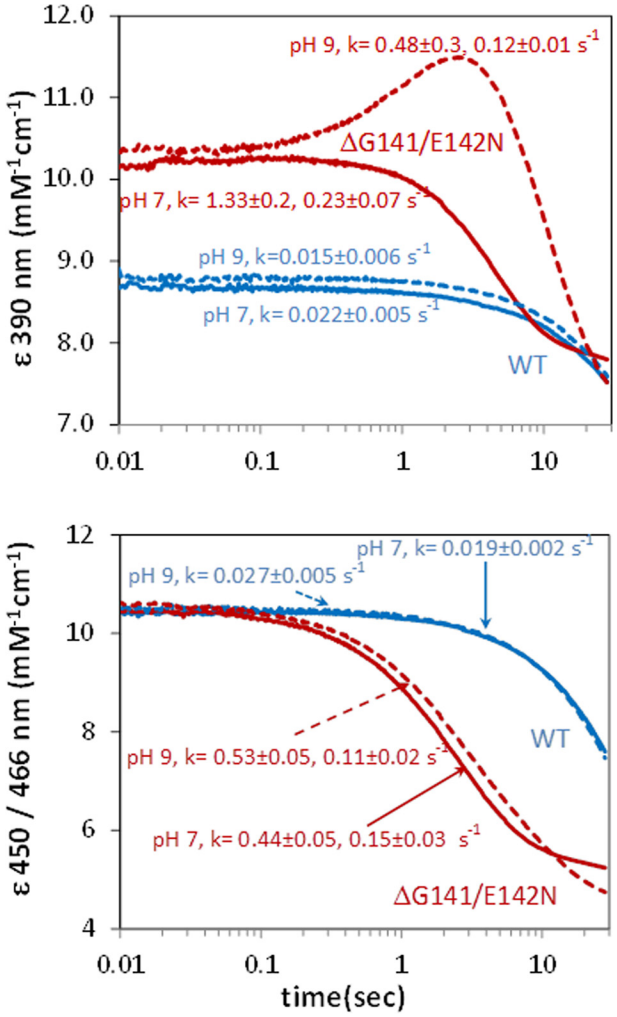

FIGURE 12. **Comparison of the rate of reduction of the FMN domain of WT and ΔG141/E142N at pH 7 and 9.** Absorbance changes at 390 and 450–466 nm during the reduction of the WT (*blue solid line*, pH 7; *blue dotted line*, pH 9) and mutant (*red solid line*, pH 7; *red dotted line*, pH 9) by 10 molar eq of $Na_2S_2O_4$ are illustrated. The final concentration after mixing at 25 °C was 5 μM FMN domain, 50 μM Na_2S_2O4, 100 mM potassium phosphate buffer, 15% glycerol. Each trace is the average of three individual traces.

The greater the amount of net negative charge on the anionic flavin, the more negative the oxidized/semiquinone couple will be and the lower its pK_a value. Examples include the WT P450 BM3 reductase and the ΔGly-141 mutants.

The high turnover rate of the ΔGly-141 mutants with cyt *c* under aerobic conditions (88/s/nmol of CYPOR) can be explained by the fact that the reaction is thermodynamically ($\Delta \cong +500$ mV) very favorable and occurs without a significant reorganization energy. Furthermore, cyt *c* reduction occurs 2–3 orders of magnitude faster (~90/s, Table 8) than the reaction of the mutants with oxygen ($k = 0.15$ s^{-1} and 0.026 s^{-1} for ΔGly-141 and ΔG141/E142N, respectively) (Tables 9 and 10). Presumably, both the semiquinone and hydroquinone are able to reduce cyt *c*. The biochemical basis for the inability of the ΔGly-141 mutants to support cyt P450 2B4 catalysis is more complex. The inactivity with cyt P450 may be either partially or completely a consequence of the following: 1) a thermodynamically unfavorable hydroquinone that appears to exist long enough to react with P450 (see below); 2) the altered structure and dynamics of the 140s loop in addition to its effect on altering the redox potential. In flavodoxins it has been observed that in the hydroquinone form the corresponding loop and active site residues are more flexible than those in the semiquinone form (69, 70). The decreased flexibility in the active site loops in the semiquinone would be advantageous for docking to a single redox partner for reduction (as in the case of P450 BM3), although a more dynamic plastic interaction surface in the hydroquinone could facilitate donation of electrons to a variety of electron-acceptor partners (as in the case of CYPOR with its numerous partners), and 3) the instability of the thermodynamically competent mutant semiquinones in oxygen relative to the rate of the sequential delivery of two electrons to cyt P450. The rate of reduction of P450 2B4 by the WT enzyme is ≅6.7 s^{-1} (37) compared with the rapid reduction of the WT and mutants by excess NADPH ($k \cong 61$, $k \cong 82.4$ s^{-1}, respectively) (Tables 6 and 7 and Figs. 9 and 10) and slower autoxidation at $k = 0.15$ and 0.026 s^{-1} for ΔGly-141 and ΔG141/E142N, respectively. These values should be sufficient to stabilize the thermodynamically incompetent hydroquinone reductase. In contrast, the short lifetime of the thermodynamically competent semiquinone would be inadequate to support P450 catalysis in the presences of excess NADPH and oxygen, if the mutant reductases function under turnover conditions in the same manner as the wild type.

The ΔGly-143 mutant retains ≅62% of the wild type activity, corrected for flavin content (Table 8), with cyt *c*. The slightly slower reaction with cyt *c* is a balance between steric hindrance and/or the marked flexibility of the 140s loop (which impedes stable H-bond formation between the flavin N5H and the carbonyl of Gly-141), and the facilitation of the reaction by the slightly greater thermodynamic driving force from the mutant reductase. In the presence of excess NADPH, under steady-state turnover conditions, ΔGly-143 should exist primarily as the hydroquinone (−297 mV) with a lower potential compared with the WT hydroquinone (−252 mV), because reduction of ΔGly-143 by NADPH ($k \cong 42$ s^{-1}, Table 7) is faster than hydroquinone oxidation in the intact protein ($k = 2.65$ s^{-1}) (Tables 9 and 10 and Fig. 11). Moreover, the semiquinone also has a potential (−235 mV) that in theory could reduce substrate-bound cyt P450 (approximately −245 mV) and support catalysis.

So why is the ΔGly-143 mutant only ~20% as active as the wild type with cyt P450? One factor is the short lifetime of the two thermodynamically competent forms of the reduced flavin in the presence of oxygen compared with the significantly slower reduction of cyt P450 2B4 (6.7 s^{-1}). The altered structure of the 140s loop as well as its flexibility may interfere with its specific binding to and reduction of ferric and oxyferrous cyt P450. Recall that reduction of cyt P450 occurs at two temporally and chemically separated steps in the catalytic cycle allowing more time for unproductive process to occur in the reductase. The greater activity of ΔGly-143 with cyt *c* (62% of WT) compared with cyt P450 (20% of WT) may also reflect a less stringent steric requirement for a productive cyt *c* reaction than the cyt P450 reaction.

Not only are the stability of the semiquinone and the redox potential critical but the dynamics and structure of the loop are

key modulators of the interaction with its redox partners as shown by the ΔGly-143 mutant. Comparison of the stability of the red semiquinones of the ΔGly-141 mutants with those of the corresponding loop in cyt P450 BM3 and the nNOS ΔGly-810 mutant at pH 9 revealed that the ΔGly-141 red semiquinones are much less stable than those of the nNOS mutant and cyt P450 BM3 (25, 68). Although the overall structures of the loops are similar, the microenvironment of the flavins is unique in each protein. There are differences in the amino acids in the loop (His-539 in BM3 replaces Asp-144 in CYPOR; Phe-809 in nNOS corresponds to Tyr-140 in CYPOR) and the residues flanking the loop also vary (Table 3). It should also be noted that two prolines flank the carboxyl terminus of the analogous loop in nNOS and cyt P450 BM3, although there is only one proline in CYPOR (Table 3). Mutations of the prolines in cyt P450 BM3 indicated that they influenced the kinetics of the flavin N5 interaction with the protein backbone. In fact, the P450 BM3 reductase P541A mutant, which corresponds to Thr-146 in CYPOR, was reduced by dithionite ~10-fold faster than the WT, although its redox potential was similar to that of the WT (36). This example is consistent with the notion that the dynamics of the loop modulates the strength of the interaction between the protein backbone and the flavin.

Comparison of the structures of the 140s loop in all four CYPOR reductases in both the oxidized and reduced states clearly demonstrates the structural basis of variable stability of the FMN blue semiquinone. Two critical changes occur upon reduction of the wild type protein. When reduced, the N5 of the flavin becomes protonated and subsequently forms a strong H-bond with the carbonyl of Gly-141. In the ΔGly-141 mutants, the flavin N5 in the oxidized protein acts as an H-bond acceptor from the amino acid amide now at position 141. This precludes protonation of N5 upon reduction and results in the formation of an unstable red anionic low potential semiquinone. In contrast, in the ΔGly-143 mutant a very flexible loop is formed that transiently allows protonation and weak H-bond formation with the protein. This results in a low potential and unstable neutral semiquinone, which upon deprotonation forms an instantaneously oxidized red semiquinone. Analysis of the eight reductase structures indicates that reduction and protonation of the flavin N5 and its subsequent stabilization by an H-bond is a major determinant of the function of the protein. For example, in the ΔGly-141 mutants, only an unstable anionic semiquinone, whose actual potential maybe more negative than that measured, is observed. In the ΔGly-143 protein, a transient blue semiquinone is formed by an unstable H-bond with a flexible 140s loop. In the wild type, the flavin N5 is protonated and stabilized by a strong H-bond with a carbonyl of the adjacent 140s loop.

In summary, the structure and dynamics of the 140s loop are major determinants of the redox potential and stability of both the semiquinone and hydroquinone of CYPOR, which in turn is critical to the catalytic and electron transfer properties of the protein. In humans, the promiscuous reductase provides electrons to ~50 different P450s, in addition to non-P450 proteins, including heme oxygenases. The autoxidation studies suggest that a stable blue semiquinone allows the CYPOR hydroquinone to function in an oxygen-containing environment while transferring one electron at a time to a two-electron-requiring process that involves many different electron acceptors. A physiological benefit of a flavin semiquinone that reacts very sluggishly with oxygen is prevention of the undesirable loss of reducing equivalents that would result from semiquinone oxidation to the quinone, resulting in reactive oxygen species generation.

Author Contributions—L. W., J.-J. P. K., F. R., S. I., C. X., M. M. H., and D. J. S. participated in research design. C. X., F. R., S. I., and M. M. H. conducted the experiments. F. R., C. X., L. W., J.-J. P. K., M. M. H., and D. J. S. performed data analysis. J.-J. P. K., L. W., F. R., C. X., M. M. H., D. J. S., and S. I. wrote or contributed to writing the manuscript.

Acknowledgments—We thank the staff at the Advanced Photon Source beamlines SBC 19ID for their assistance in data collection.

References

1. Massey, V., and Hemmerich, P. (1980) Active-site probes of flavoproteins. *Biochem. Soc. Trans.* **8,** 246–257
2. Røhr, A. K., Hersleth, H.-P., and Andersson, K. K. (2010) Tracking flavin conformations in protein crystal structures with Raman spectroscopy and QM/MM calculations. *Angew. Chem. Int. Ed. Engl.* **49,** 2324–2327
3. Cui, D., Koder, R. L., Jr., Dutton, P. L., and Miller, A.-F. (2011) ^{15}N solid-state NMR as a probe of flavin H-bonding. *J. Phys. Chem. B* **115,** 7788–7798
4. Evans, E. W., Dodson, C. A., Maeda, K., Biskup, T., Wedge, C. J., and Timmel, C. R. (2013) Magnetic field effects in flavoproteins and related systems. *Interface Focus* **3,** 20130037
5. Miura, R. (2001) Versatility and specificity in flavoenzymes: control mechanisms of flavin reactivity. *Chem. Rec.* **1,** 183–194
6. Ghisla, S., and Massey, V. (1989) Mechanisms of flavoprotein-catalyzed reactions. *Eur. J. Biochem.* **181,** 1–17
7. Senda, T., Senda, M., Kimura, S., and Ishida, T. (2009) Redox control of protein conformation in flavoproteins. *Antioxid. Redox Signal.* **11,** 1741–1766
8. Ghisla, S., and Massey, V. (1986) New flavins for old: artificial flavins as active site probes of flavoproteins. *Biochem. J.* **239,** 1–12
9. Mayhew, S. G. (1999) The effects of pH and semiquinone formation on the oxidation-reduction potentials of flavin mononucleotide: a reappraisal. *Eur. J. Biochem.* **265,** 698–702
10. Iyanagi, T., Xia, C., and Kim, J. J. (2012) NADPH-cytochrome P450 oxidoreductase: prototypic member of the diflavin reductase family. *Arch. Biochem. Biophys.* **528,** 72–89
11. Breinlinger, E. C., Keenan, C. J., and Rotello, V. M. (1998) Modulation of flavin recognition and redox properties through donor atom-π interactions. *J. Am. Chem. Soc.* **120,** 8606–8609
12. Koziol, L., Kumar, N., Wong, S. E., and Lightstone, F. C. (2013) Molecular recognition of aromatic rings by flavin: electrostatics and dispersion determine ring positioning above isoalloxazine. *J. Phys. Chem. A* **117,** 12946–12952
13. Paine, M. J., Scrutton, N. S., Munro, A. W., Gutierrez, A., Roberts, G. C. K., and Wolf, C. R. (2005) in *Cytochrome P450* (Ortiz de Montellano, P. R., ed) 3rd Ed., pp. 115–148, Kluwer Academic/Plenum Publishers, New York
14. Ortiz de Montellano, P. R. (2010) Hydrocarbon hydroxylation by cytochrome P450 enzymes. *Chem. Rev.* **110,** 932–948
15. Guengerich, F. P. (2005) in *Cytochrome P450: Structure, Mechanism and Biochemistry* (Ortiz de Montellano, P. R., ed.) 3rd Ed., pp. 377–463, Kluwer Academic/Plenum Publishers, New York.
16. Guengerich, F. P. (2015) in *Cytochrome P450: Structure, Mechanism and Biochemistry* (Ortiz de Montellano, P. R., ed) 4th Ed., pp. 523–785, Springer International Publishers, Switzerland
17. Im, S. C., and Waskell, L. (2011) The interaction of microsomal cyto-

chrome P450 2B4 with its redox partners, cytochrome P450 reductase and cytochrome *b*5. *Arch. Biochem. Biophys.* **507,** 144–153
18. Schacter, B. A., Nelson, E. B., Marver, H. S., and Masters, B. S. (1972) Immunochemical evidence for an association of heme oxygenase with the microsomal electron transport system. *J. Biol. Chem.* **247,** 3601–3607
19. Guengerich, F. P. (2005) Reduction of cytochrome *b*5 by NADPH-cytochrome P450 reductase. *Arch. Biochem. Biophys.* **440,** 204–211
20. Oprian, D. D., and Coon, M. J. (1982) Oxidation-reduction states of FMN and FAD in NADPH-cytochrome P-450 reductase during reduction by NADPH. *J. Biol. Chem.* **257,** 8935–8944
21. Vermilion, J. L., Ballou, D. P., Massey, V., and Coon, M. J. (1981) Separate roles for FMN and FAD in catalysis by liver microsomal NADPH-cytochrome P-450 reductase. *J. Biol. Chem.* **256,** 266–277
22. Porter, T. D., and Kasper, C. B. (1986) NADPH-cytochrome P450 oxidoreductase: flavin mononucleotide and flavin adenine dinucleotide domains evolved from different flavoproteins. *Biochemistry* **25,** 1682–1687
23. Sevrioukova, I., Shaffer, C., Ballou, D. P., and Peterson, J. A. (1996) Equilibrium and transient state spectrophotometric studies of the mechanism of reduction of the flavoprotein domain of P450 BM3. *Biochemistry* **35,** 7058–7068
24. Sevrioukova, I. F., Li, H., Zhang, H., Peterson, J. A., and Poulos, T. L. (1999) Structure of a cytochrome P450-redox partner electron-transfer complex. *Proc. Natl. Acad. Sci. U.S.A.* **96,** 1863–1868
25. Li, H., Das, A., Sibhatu, H., Jamal, J., Sligar, S. G., and Poulos, T. L. (2008) Exploring the electron transfer properties of neuronal nitric-oxide synthase by reversal of the FMN redox potential. *J. Biol. Chem.* **283,** 34762–34772
26. Wang, M., Roberts, D. L., Paschke, R., Shea, T. M., Masters, B. S., and Kim, J. J. (1997) Three-dimensional structure of NADPH-cytochrome P450 reductase: prototype for FMN- and FAD-containing enzymes. *Proc. Natl. Acad. Sci. U.S.A.* **94,** 8411–8416
27. Hubbard, P. A., Shen, A. L., Paschke, R., Kasper, C. B., and Kim, J. J. (2001) NADPH-cytochrome P450 oxidoreductase. Structural basis for hydride and electron transfer. *J. Biol. Chem.* **276,** 29163–29170
28. Xia, C., Panda, S. P., Marohnic, C. C., Martásek, P., Masters, B. S., and Kim, J.-J. (2011) Structural basis for human NADPH-cytochrome P450 oxidoreductase deficiency. *Proc. Natl. Acad. Sci. U.S.A.* **108,** 13486–13491
29. Munro, A. W., Noble, M. A., Robledo, L., Daff, S. N., and Chapman, S. K. (2001) Determination of the redox properties of human NADPH-cytochrome P450 reductase. *Biochemistry* **40,** 1956–1963
30. Zhou, Z., and Swenson, R. P. (1995) Electrostatic effects of surface acidic amino acid residues on the oxidation-reduction potentials of the flavodoxins from *Desulfovibrio vulgaris.* (Hildenborough). *Biochemistry* **34,** 3183–3192
31. O'Farrell, P. A., Walsh, M. A., McCarthy, A. A., Higgins, T. M., Voordouw, G., and Mayhew, S. G. (1998) Modulation of the redox potentials of FMN in *Desulfovibrio vulgaris* flavodoxin: thermodynamic properties and crystal structures of glycine-61 mutants. *Biochemistry* **37,** 8405–8416
32. Garcin, E. D., Bruns, C. M., Lloyd, S. J., Hosfield, D. J., Tiso, M., Gachhui, R., Stuehr, D. J., Tainer, J. A., and Getzoff, E. D. (2004) Structural basis for isozyme-specific regulation of electron transfer in nitric-oxide synthase. *J. Biol. Chem.* **279,** 37918–37927
33. Hoover, D. M., Drennan, C. L., Metzger, A. L., Osborne, C., Weber, C. H., Pattridge, K. A., and Ludwig, M. L. (1999) Comparisons of wild type and mutant flavodoxins from *Anacystis nidulans.* Structural determinants of the redox potentials. *J. Mol. Biol.* **294,** 725–743
34. Ludwig, M. L., Pattridge, K. A., Metzger, A. L., Dixon, M. M., Eren, M., Feng, Y., and Swenson, R. P. (1997) Control of oxidation-reduction potentials in flavodoxin from *Clostridium beijerinckii:* The role of conformation changes. *Biochemistry* **36,** 1259–1280
35. Watt, W., Tulinsky, A., Swenson, R. P., and Watenpaugh, K. D. (1991) Comparison of the crystal structures of a flavodoxin in its three oxidation states at cryogenic temperatures. *J. Mol. Biol.* **218,** 195–208
36. Kasim, M., Chen, H. C., and Swenson, R. P. (2009) Functional characterization of the re-face loop spanning residues 536–541 and its interactions with the cofactor in the flavin mononucleotide-binding domain of flavocytochrome P450 from Bacillus megaterium. *Biochemistry* **48,** 5131–5141
37. Hamdane, D., Xia, C., Im, S. C., Zhang, H., Kim, J. J., and Waskell, L. (2009) Structure and function of an NADPH-cytochrome P450 oxidoreductase in an open conformation capable of reducing cytochrome P450. *J. Biol. Chem.* **284,** 11374–11384
38. Miroux, B., and Walker, J. E. (1996) Over-production of proteins in *Escherichia coli*: mutant hosts that allow synthesis of some membrane proteins and globular proteins at high levels. *J. Mol. Biol.* **260,** 289–298
39. Kurzban, G. P., and Strobel, H. W. (1986) Preparation and characterization of FAD-dependent NADPH-cytochrome P-450 reductase. *J. Biol. Chem.* **261,** 7824–7830
40. Saribas, A. S., Gruenke, L., and Waskell, L. (2001) Overexpression and purification of the membrane-bound cytochrome P450 2B4. *Protein Expr. Purif.* **21,** 303–309
41. Bridges, A., Gruenke, L., Chang, Y. T., Vakser, I. A., Loew, G., and Waskell, L. (1998) Identification of the binding site on cytochrome P450 2B4 for cytochrome *b*5 and cytochrome P450 reductase. *J. Biol. Chem.* **273,** 17036–17049
42. Dutton, P. L. (1978) Redox potentiometry: determination of midpoint potentials of oxidation-reduction components of biological electron-transfer systems. *Methods Enzymol.* **54,** 411–435
43. Chen, H. C., and Swenson, R. P. (2008) Effect of the insertion of a glycine residue into the loop spanning residues 536–541 on the semiquinone state and redox properties of the flavin mononucleotide-binding domain of flavocytochrome P450BM-3 from *Bacillus megaterium*. *Biochemistry* **47,** 13788–13799
44. McPherson, A. (1999) *Crystallization of Biological Macromolecules*, Cold Spring Harbor Laboratory Press, Cold Spring Harbor, New York
45. Otwinowski, Z., and Minor, W. (1997) Processing of X-ray diffraction data collected in oscillation mode. *Methods Enzymol.* **276,** 307–326
46. Brunger, A. T. (2007) *The Crystallography and NMR System.* Version 1.2. *Nat. Protoc.* **2,** 2728–2733
47. Emsley, P., and Cowtan, K. (2004) Coot: Model-building Tool for Molecular Graphics. *Acta Crystallogr. D Biol. Crystallogr.* **60,** 2126–2132
48. Xia, C., Hamdane, D., Shen, A. L., Choi, V., Kasper, C. B., Pearl, N. M., Zhang, H., Im, S. C., Waskell, L., and Kim, J. J. (2011) Conformational changes of NADPH-cytochrome P450 oxidoreductase are essential for catalysis and cofactor binding. *J. Biol. Chem.* **286,** 16246–16260
49. Hutchinson, E. G., and Thornton, J. M. (1994) A revised set of potentials for β-turn formation in proteins. *Protein Sci.* **3,** 2207–2216
50. Luschinsky, C. L., Dunham, W. R., Osborne, C., Pattridge, K. A., and Ludwig, M. L. (1991) in *Flavins and Flavoproteins* (Curti, B. S., Ronchi, S., and Zanetti, G., eds) pp. 409–413, Walter de Gruyter, Berlin
51. Chang, F. C., and Swenson, R. P. (1999) The midpoint potentials for the oxidized-semiquinone couple for GLY57 mutants of the *Clostridium beijerinckii* flavodoxin correlate with changes in the hydrogen-bonding interaction with the proton on N(5) of the reduced flavin mononucleotide cofactor as measured by NMR chemical shift temperature dependencies. *Biochemistry* **38,** 7168–7176
52. Goñi, G., Serrano A., Frago, S., Hervás, M., Peregrina J. R., De la Rosa, M. A., Gómez-Moreno, C., Navarro, J. A., and Medina, M. (2008) Flavodoxin-mediated electron transfer from photosystem I to ferredoxin-$NADP^+$ reductase in anabaena: role of flavodoxin hydrophobic residues in protein-protein interactions. *Biochemistry* **47,** 1207–1217
53. Deane, C. M., Allen, F. H., Taylor, R., and Blundell, T. L. (1999) Carbonyl-carbonyl interactions stabilize the partially allowed Ramachandran conformations of asparagine and aspartic acid. *Protein Eng.* **12,** 1025–1028
54. Yang, A. S., Hitz, B., and Honig, B. (1996) Free energy determinants of secondary structure formation: III. β-turns and their role in protein folding. *J. Mol. Biol.* **259,** 873–882
55. Johansson L. B., Davidsson, A., Lindblom, G., and Naqvi, K. R. (1979) Electronic transitions in the isoalloxazine ring and orientation of the flavin in the model membranes studied by polarized light spectroscopy. *Biochemistry* **18,** 4249–4253
56. Nishimoto, K., Watanabe, Y., and Yagi, K. (1978) Hydrogen bonding of flavoprotein. I. Effect of hydrogen bonding on electronic spectra of flavoprotein. *Biochim. Biophys. Acta.* **526,** 34–41
57. Iyanagi, T., Makino, N., and Mason, H. S. (1974) Redox properties of the reduced nicotinamide adenine dinucleotide phosphate-cyto-

chrome P-450 and reduced nicotinamide adenine dinucleotide-cytochrome b_5 reductases. *Biochemistry* **13,** 1701–1710
58. Das, A., and Sligar, S. G. (2009) Modulation of the cytochrome P450 reductase redox potential by the phospholipid bilayer. *Biochemistry* **48,** 12104–12112
59. Wolthers, K. R., Basran, J., Munro, A. W., and Scrutton, N. S. (2003) Molecular dissection of human methionine synthase reductase: determination of the flavin redox potentials in full-length enzyme isolate flavin-binding domains. *Biochemistry* **42,** 3911–3920
60. Zhang, H., Gruenke, L., Arscott, D., Shen, A., Kasper, C., Harris, D. L., Glavanovich, M., Johnson, R., and Waskell, L. (2003) Determination of the rate of reduction of oxyferrous cytochrome P450 2B4 by 5-deazaFAD T491V cytochrome P450 reductase. *Biochemistry* **42,** 11594–11603
61. Draper, R. D., and Ingraham, L. L. (1968) A potentiometric study of the flavin semiquinone equilibrium. *Arch. Biochem. Biophys.* **125,** 802–808
62. Anderson, R. F. (1983) Energetics of the one-electron reduction steps of riboflavin, FMN and FAD to their fully reduced forms. *Biochim. Biophys. Acta* **722,** 158–162
63. Sevrioukova, I., Truan, G., and Peterson, J. A. (1996) The flavoprotein domain of P450 BM3: expression, purification, and properties of the flavin adenine dinucleotide- and flavin mononucleotide-binding subdomains. *Biochemistry* **35,** 7528–7535
64. Shen, A. L., Porter, T. D., Wilson, T. E., and Kasper, C. B. (1989) Structural analysis of the FMN binding domain of NADPH-cytochrome P-450 oxidoreductase by site-directed mutagenesis. *J. Biol. Chem.* **264,** 7584–7589
65. Massey, V. (1994) Activation of molecular oxygen by flavins and flavoproteins. *J. Biol. Chem.* **269,** 22459–22462
66. Edmondson, D. E., Barman, B., and Tollin, G. (1972) On the importance of the N-5 position in flavin coenzymes, properties of free and protein-bound 5-deaza analogs. *Biochemistry* **11,** 1133–1138
67. Massey, V. (2002) The reactivity of oxygen with flavoproteins. *International Congress Series* **1233,** 3–11
68. Hanley, S. C., Ost, T. W., and Daff, S. (2004) The unusual redox properties of flavocytochrome P450 BM3 flavodoxin domain. *Biochem. Biophys. Res. Commun.* **325,** 1418–1423
69. Chang, C. W., He, T. F., Guo, L., Stevens, J. A., Li, T., Wang, L., and Zhong, D. (2010) Mapping solvation dynamics at the function site of flavodoxin in three redox states. *J. Am. Chem. Soc.* **132,** 12741–12747
70. Leenders, R., van Gunsteren, W. F., Berendsen, H. J., and Visser, A. J. (1994) Molecular dynamics simulations of oxidized and reduced *Clostridium beijerinckii* flavodoxin. *Biophys. J.* **66,** 634–645